MOVING LOAD BRIDGE MONITORING BY OPTIMUM FILTER

Pedro Alba de la Rubia
Ingeniero Industrial

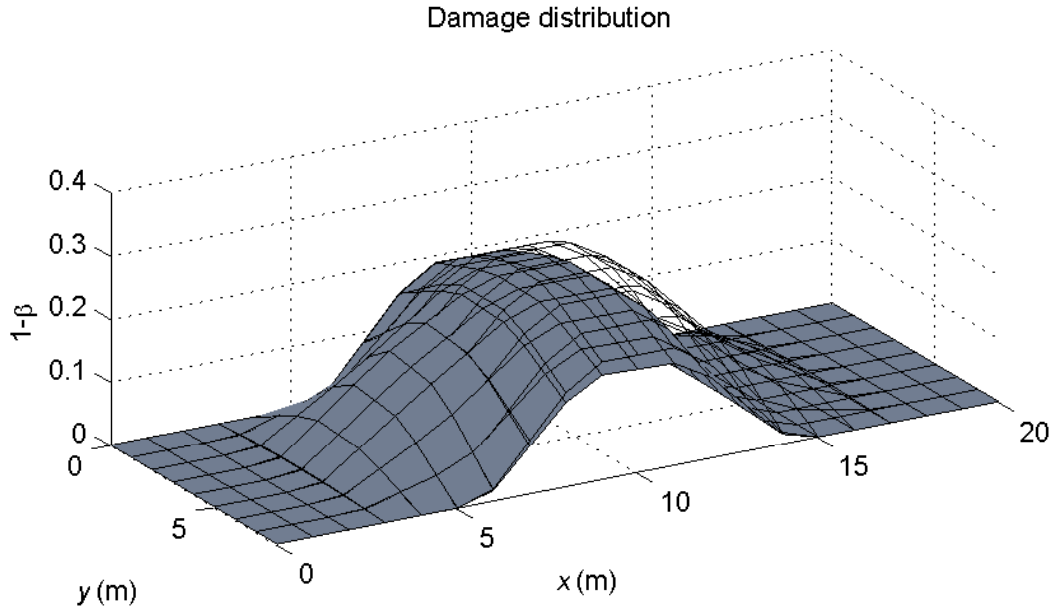

Contents

1. Abstract

The purpose of this work is to reconstruct the damage distribution in plate bridge decks from noisy response data from moving loads, using a minimization scheme of the discrepancy between measurements and simulations. A linear stiffness degradation continuum damage model is used, together with a first order shear deformation theory (FSDT), to predict the structural behavior and to detect damage from noisy measurements. The effects of noise associated with the uncertainty of measurements due to the complex nature of the damage-deck-moving load interactions are considered for different bridge geometries, moving load speed and deck thickness/length ratios.

Genetic algorithms have been used to minimize the cost function. A local interpolation model has been implemented to reconstruct the damage. Several numerical results show that the inversion algorithm is computationally efficient in reconstructing stiffness degradation for this kind of structures. The propose inverse problem strategy reconstructs the defect characteristics with sufficient precision, under realistic levels of noise.

The new contributions consist in a new parameterization of the spatial distribution of damage, a new formulation of the semi-analytical estimate of the probability of detection, a inverse problem based on type of mobile load on bridge decks, the filter optimization and position measurement using as criteria the POD and a parametric study of how it affects the design of the bridge and the loads. In this work some of the knowledge acquired during the completion of the master structures have been implemented, also the architecture of inverse problems based on models have been learned.

Keywords:

Inverse problem, damage identification, moving load, bridge deck, finite element method, genetic algorithms.

2. Introduction

Recently, some investigaters started turning their attention to the damage detection by solving the inverse problem from static or dynamic responses obtained by the forward procedure. Direct search methods, such as neural networks, genetic algorithms and simulated annealing methods are developed and promisingly applied to the field of structural identification. Among them, genetic algorithms (GA) attract our attention because of the fact that the technique requires significantly small amount of data in dealing with complex problems, while attaining global convergence as opposed to gradient-based methods. Suh *et al.* [32] presented a hybrid neuro-genetic technique that is able to identify the location and extent of damage in a beam or frame structure using only the frequency information. Mares and Surace [21] demonstrated the ability of the GA to identify damage in elastic structures. Friswell *et al.* [5] combined the genetic and eigen-sensitivity algorithms for locating damage.

Chou and Ghaboussi [4] proposed a GA-based method to determine the location and extent of damage in truss structures from the measured static displacements. Krawczuk [12] presented a wave propagation approach to detect damage in beam structures based on GA and a gradient-based technique. However, all these works are limited in that they can analyze only structural members made of isotropic materials. Recently, techniques for detecting damages from noisy static or dynamic responses of anisotropic plates are evolving. Lee and Wooh [17] applied an advanced micro-genetic algorithm for detecting damage of steel and composite structures subjected to dynamic loading. Rus *et al.* [28] dealt with a method of damage detection for plane stress problem of composites using boundary element method (BEM). Lee and Wooh [16] applied the micro-genetic algorithm for detections stiffness reduction of composite plates based on the high order shear deformation theory (HSDT).

Despite the broad spectrum of applications for detecting damage, the numerical techniques may not be attractive from the practical point of view. The methods require a precise measurement of static or moving loading to the structure that needs to be input into the numerical model. Based on experimental work, precise control and measurement of input loading are extremely difficult because of errors (noisy responses) arising from the structural behaviour, ambient and measuring devices. In order to solve the inverse problem of structure with noisy data, the conventional techniques usually require a large number of iterations, and thus, a high computational cost. Therefore, an effective reduction of the noise may be significant issue for faster convergence, better computational efficiency and more precise and sensitive detection.

In order to reduce the noise effect in the dynamic response data, this study is focused on an efficient fitering algorithm based on the wavelet transform. The wavelet

transform is a technique for the processing of signals whose spectral countenance is non-stationary. It is defined in terms of a base function, and obtained by compression, dilatation and decay operations of the mother wavelet. In the wavelet transform, the signal spectrum is divided by an overlapping of pass band filters with constant relative bandwidth. Addison [1] gives an excellent overview of the potential that the novel wavelet analysis provides to different areas of science in the current days. Within the subject of mechanical systems, Kim [11] gives a successfull wavelet ridge analysis of the correlation of reflected to incident wave magnitude ratio over the time and frequency to correlate an experiment with a bending beam model.

This application is merged with numerical methods by Li *et al.* [19] who use the wavelet finite element method (WFEM) in modal analysis to find cracks with the aim of solving accurately the crack singularities. On the other hand, wavelets can also be used for noise removal, which is our objective in this study. Messina *et al.* [22] compares wavelets for noise removal against differentiator filters, concluding that they provide similar performance. In a similar approach, Yang *et al.* [35] apply envelope complex wavelet analysis correlation to efficiently discriminate noise from the signals in an experimental case. In this study, a standard wavelet analysis is used as a filtering tool within a novel framework of optimization of the search methodology.

In standard practice of nondestructive evaluation (NDE), the issue of the probability of detection (POD) has only been addressed independently, under the name of identifiability, in statistics and mathematics, with a wide application in chemistry and physics. However, in the field of nondestructive testing, only observational comments have been made. Only Liu *et al.* [20] discussed as identifiability the relationship between the number of measurements and the number of degrees of freedom to establish a necessity condition. Tarantola *et al.* [33] examined the inversion theory under a probabilistic formulation and introduced probability density functions in the model and the a priori information about the parameters to explain the robustness of the inversion and to obtain a non-single valued output for the parameters. In this study, an estimate of the POD is designed from the minimization search approach as a criteria to be optimized for the design of the formulation.

The forward and inverse procedures are presented for the identification of stiffness degradation in bridge deck plates by combining the FEM as the numerical procedure for the simulation of the effect of the defect on the response to moving loads. A filter is introduced that weights the wavelet coefficients, time windows and measurement points. Then, the POD is approximated from certain simulated values of the measurements. Finally, the proposed method determines the best measuring points, wavelets levels and time windows for locating and evaluating stiffness degradation on the deck. A parametric study is carried out for different bridge geometries, moving load speed and deck thickness/length ratios.

3. Methodology

The problem of nondestructive damage recontruction is solved by a model-based inverse problem approach that consists of two step: (i) to excite the system applying moving load, and (ii) to measure the response (displacements). A finite element method model is used in the forward procedure that is explained in detail in the next section. The elements that play in the IP are summarized in Figure 1, and are explained in detail in this section.

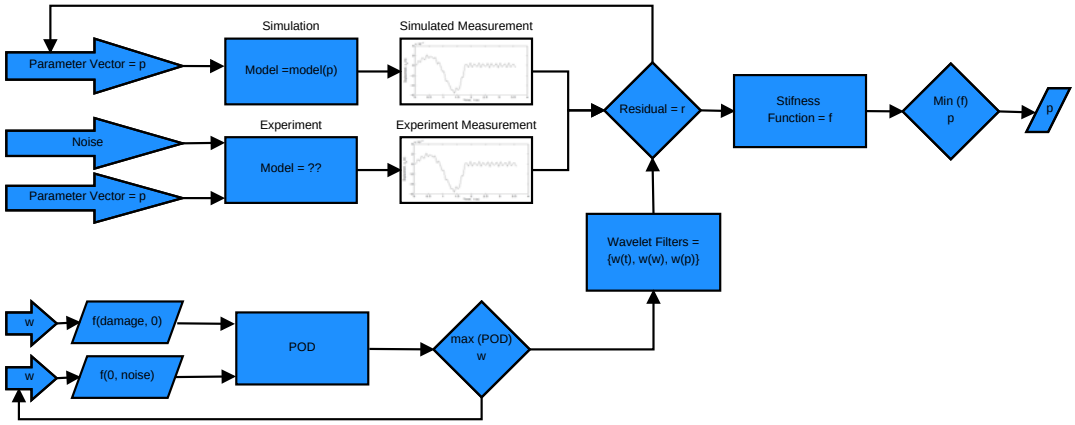

Figure 1. Issues squeme for the solution of the model-based Inverse Problem.

3.1. Forward procedure

3.1.1. Finite element method model with degraded element In the finite element formulation, the stiffness matrix of the kth damaged element in the local coordinates can now be written as the volume integral form, that is

$$\tilde{\mathbf{K}}^{(m)} = \tilde{\beta}^{(m)}(\xi^{(k)})\mathbf{K}^{(m)} \tag{1}$$

where $\xi^{(k)}$ is the coordinate vector of kth element; and ($\mathbf{K}^{(m)} = \int_V \mathbf{B}^{(e)T}\mathbf{D}^{(m)}\mathbf{B}^{(e)}\,dV$) is the stiffness matrix at the mth element of a plate. Note that $\mathbf{K}^{(m)}$ is a property that is independent of damage; thus it is applicable to all the elements (e), whether damaged or not.

The governing equation of motion of the system using Eq. 1 is written in the form

$$\mathbf{M}\ddot{\mathbf{U}} + \tilde{\mathbf{K}}\mathbf{U} = \bar{\mathbf{F}}(t) \tag{2}$$

where $\mathbf{U}$ and $\ddot{\mathbf{U}}$ are the displacement and acceleration vectors, respectively; $\mathbf{M}$ is the mass matrix without loss before and after damage; $\tilde{\mathbf{K}}$ is the stiffness reduction matrix; and $\bar{\mathbf{F}}(t)$ is the time history of the applied load.

For the transient analysis of a slab bridge subjected to the effects of moving loads, Newmark's explicit integration technique is adopted by Bathe *et al.* [3]. Considering a moving load with a velocity v on a plate element, the total moving distance ($^{t+\Delta t}D_t$) of the load at time $t+\delta t$ is given by

$$^{t+\Delta t}D_t = \frac{v\Delta t}{3.6} + C_{x_1} \tag{3}$$

where C_{x_1} denotes the initial coordinate of the moving load in the longitudinal direction.

The location number $\bar{I}_d$ of the element which the moving load passes through at time $t+\delta t$ can be expressed as

$$^{t+\Delta t}\bar{I}_d = N^d_{x_2} I_1 + I_s + 1 \tag{4}$$

where

$$I_1 = INT\left(\frac{^{t+\Delta t}D_t N^d_{x_1}}{L_{x_1}}\right), \qquad I_s = INT\left(\frac{C_{x_2} N^d_{x_2}}{L_{x_2}}\right) \tag{5}$$

and $N^d_{x_1}$ and $N^d_{x_2}$ are the number of division elements in the longitudinal (x_1) and transverse direction (x_2), respectively; C_{x_2} is the initial coordinate of the moving load in the transverse direction; L_{x_1} and L_{x_2} are the length of a plate in the x_1 and x_2 directions, respectively; and INT( ) means the integer part of the value in a parenthesis.

The moving load vectors $F_k(t)$ at an arbitrary location on the N^d_kth element of the plate should be inevitably distributed to the nodal loads $\bar{F}_{N_k}(t)$ using the zeroth-order Hermite (Lagrange) interpolation function Φ . The natural coordinates(ξ_k, η_k) of the element for the moving load at time $t+\delta t$ can be derived as

$$^{t+\Delta t}\xi_k = 2\left(\frac{[C_{x_1} + ^{t+\Delta t} D_t] N^d_{x_1}}{L_{x_1}} - I_1\right) \tag{6}$$

$$^{t+\Delta t}\eta_k = 2\left(\frac{C_{x_2}N_{x_2}^d}{L_{x_2}} - I_s\right) - 1 \tag{7}$$

In a four-node element with three degrees of freedom per node, the moving load distribution into four neighbourhood nodes not considering distribution of moment can be expressed as

$$^{t+\Delta t}\bar{\mathbf{F}}_{N_k} = \Phi^T\left(^{t+\Delta t}\xi_k, ^{t+\Delta t}\eta_k\right) F_k(t+\Delta t) \tag{8}$$

The total external force vectors $\bar{\mathbf{F}}$ applied on the plate at $t+\Delta t$ can be obtained by summing up the distributed n loads as given by

$$^{t+\Delta t}\bar{\mathbf{F}} = ^{t+\Delta t}\bar{\mathbf{F}}_{N_1} + ^{t+\Delta t}\bar{\mathbf{F}}_{N_2} + ... + ^{t+\Delta t}\bar{\mathbf{F}}_{N_n} \tag{9}$$

In Newmark integration scheme, the effective loads at time $t+\Delta t$ can be calculated as

$$^{t+\Delta t}\bar{\mathbf{F}} = ^{t+\Delta t}\bar{\mathbf{F}} + \mathbf{M}(\lambda_0^t\mathbf{U} + \lambda_2^t\dot{\mathbf{U}} + \lambda_3^t\ddot{\mathbf{U}}) \tag{10}$$

The dynamic displacements $\mathbf{U}$, accelerations $\ddot{\mathbf{U}}$, and velocities $\dot{\mathbf{U}}$ at time $t+\Delta t$ can be solved as

$$^{t+\Delta t}\mathbf{U} = \hat{\mathbf{K}}^{-1}(^{t+\Delta t}\bar{\mathbf{F}})(10-a) \tag{11}$$

$$^{t+\Delta t}\ddot{\mathbf{U}} = \lambda_0(^{t+\Delta t}\mathbf{U} - ^{t}\mathbf{U}) - \lambda_2^t\dot{\mathbf{U}} + \lambda_3^t\ddot{\mathbf{U}} \tag{12}$$

$$^{t+\Delta t}\dot{\mathbf{U}} = ^{t}\dot{\mathbf{U}} - \lambda_6^t\ddot{\mathbf{U}} - \lambda_7^{t+\Delta t}\ddot{\mathbf{U}}(10-c) \tag{13}$$

where the triangularized effective stiffness matrix is $\hat{\mathbf{K}} = \tilde{\mathbf{K}} + \lambda_0\mathbf{M}$; and λ_0, λ_2 , λ_3 , λ_6 and λ_7 are integration constants in the Newmark integration method, respectively.

3.1.2. Bridge deck and moving load description The bridge deck in which the damage will be sought is defined by geometry, material, boundary conditions and measuring points. Several dimensions are proposed for the parametric study, length and thickness. The boundary conditions are supported on two opposite sides. And moving load is applied along the bridge at 40km/h - 120 km/h by the middle of the bridge, see Figure 2. The measurements are made at the four points distributed over a regular 3 x 6 mesh. The moving load has a magnitude of 10000 kg, and the measurement recording period is 3 ms.

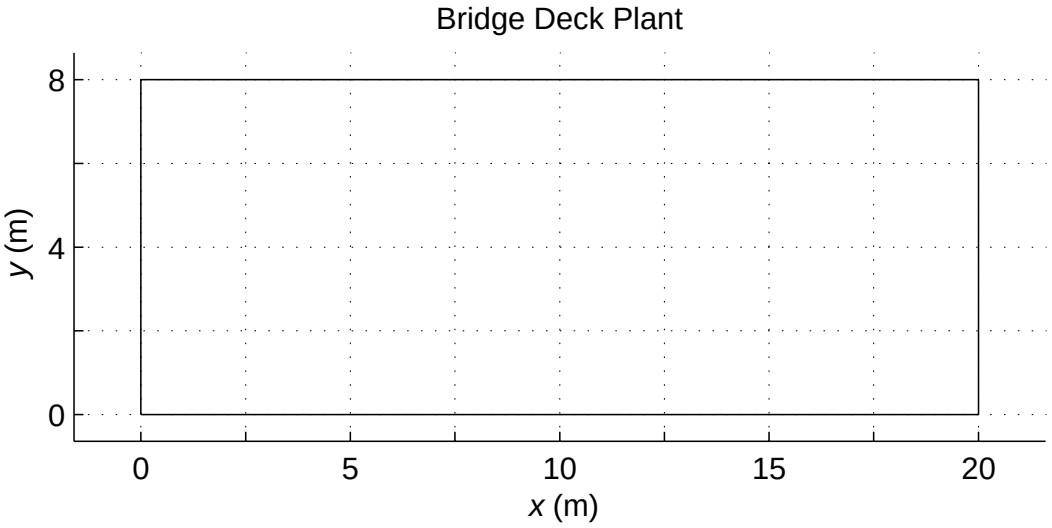

Figure 2. Bridge deck plant with dimensions 20 x 8 m.

3.1.3. Noise effect In order to consider unexpected errors in the measured displacements or accelerations, the usual option is to introduce the effects of random noise by adding Gaussian noise directly to the values computed by the FEM. Given a measured response on the kth node, a Gaussian (Normal) random number generator is used to generate a series of random numbers $\zeta_k[n]$ with standard deviation $\sigma = 1$ and zero mean, $\zeta_k[n] = N(0, 1)$. This series simulates a random process $\zeta(t)$, and the simulated measurements are given by,

$$\psi^x(p; \psi_n)[n] \simeq \psi(p)[n] + h(n) * RMS(\psi)\zeta[n] \tag{14}$$

where $RMS(\psi)$ is the root mean square given by,

$$RMS(\psi) = \sqrt{\frac{1}{N[n]} \sum_{n=1}^{N[n]} (\psi)^2} \tag{15}$$

and where $h(n)$ is the time-discretized Fourier transform of the frequency spectrum $H(\omega_j)$ of the noise, and $*$ stands for convolution product. In the following numerical experiments, only white noise (uniform frequency spectrum) is used, but in case the process is assigned a non-uniform frequency spectrum, that can be estimated during the calibration process, the following relationship can be extracted,

$$\sigma^n = \sqrt{\frac{1}{N^2}\sum_{j=0}^{N-1}|H_j|^2} \tag{16}$$

Redundant measurements are an effective way to reduce the effect of noise. If the noise is assumed Gaussian with zero mean and standard deviation σ^n, an effective way to reduce it is increasing the number of measurements N. Then, since the system is linear we can just take it into account substituting the measurements with their mean values, and the noise will reduce with a factor $\frac{1}{\sqrt{N}}$,

$$\begin{aligned}&\tilde{\psi} = \frac{1}{N}\sum_k \psi_k \quad \Rightarrow \\ &\frac{1}{N}\sum_k(\psi_k + h * \zeta_k) = \tilde{\psi} + \frac{h}{N} * \sum_k n_k = \tilde{\psi} + \frac{h}{\sqrt{N}} * \zeta\end{aligned} \tag{17}$$

A similar conclusion can be drawn, when the number of measurements is multipled by a factor N, for the ratio $\frac{f,n}{f,p}$ (defined later), which can be proved to reduce by a factor $\frac{1}{\sqrt{N}}$. More details can be found in Oppenheim [24].

3.2. Inverse procedure

The inverse procedure presented aims at characterizing damage in a structure (degree of degradation) and determine its extent and location. The testing consists of two steps: (1) to disturb a structure with a known excitation function (the moving load defined by the weight, speed and trajectory of the vehicle) and (2) to measure its response (transient time history or a waveform representing the displacements, usually obtained by accelerometers) at one or more locations in the structure. We assume that the dynamic behavior of the structure in its intact and damaged states is predictable using a well-calibrated model.

Then, the measured signal is processed to solve the *inverse problem*, i.e., to determine the changes in the structure from its original state. A genetic algorithm search tool (Lee and Wooh [16], Goldberg [7]) is used to minimize the discrepancy

between the experimental readings and the numerically predicted trial response, by means of a cost functional designed to calibrate for coherent uncertainties and noise, and providing maximal robustness and sensitivity. Thus, we focus on determining the best cost functional for detecting damage from responses with noise. We propose and optimal choice of measuring points as well as time windows and wavelet level filters for better sensitivity to noise effects. The criterion for this is chosen in a rational way so as to maximize the probability of detection.

3.2.1. Cost functional The readings from the sensors are denoted by ψ for the theoretical or synthetic case, and ψ^x for the experimental case. They do not need to coincide with the measurements Φ to analyze, which can be improved by being calibrated magnitudes, so that they gain independency from the ambient conditions during the experiment and coherent noise, and also by being adimensional. A reading $\overset{\circ}{\psi}$ in the undamaged state of the specimen is defined for calibration, and the measurement to analyze is defined as,

$$\Phi = \frac{\psi - \overset{\circ}{\psi}}{RMS(\overset{\circ}{\psi})} \tag{18}$$

where the RMS values are defined for a discrete function f in time domain $f(t_i)$ or frequency domain $F(\omega_j)$ at N sampling points as,

$$RMS(f) = \sqrt{\frac{1}{N}\sum_{i=0}^{N-1} f(t_i)^2} = \sqrt{\frac{1}{N^2}\sum_{j=0}^{N-1} |F(\omega_j)|^2} \tag{19}$$

A residual γ is defined from the misfit or discrepancy $\Phi^x - \Phi$ between the measurements. A filter w is included, which will be later defined for optimizing the residual,

$$\gamma = w(\Phi^x - \Phi) \tag{20}$$

The cost functional f or fitness function is defined after a residual vector γ of size N_i as the quadratic form,

$$f = \frac{1}{2}|\gamma|^2 = \frac{1}{2}\frac{1}{N_i}\sum_{i=1}^{N_i} \gamma_i^2 \tag{21}$$

It is useful to define an alternative version of the cost functional denoted as f^l, with the property of improving the sensitivity while approaching the optimum, just by introducing a logarithm and a small value ϵ to ensure its existence. This definition particularly enhances the convergence speed when the minimization is tackled by with genetic algorithms or other random search algorithms (see Rus *et al.* [6]),

$$f^l = \log(f + \epsilon) \tag{22}$$

3.2.2. Probability of detection The economy of the health monitoring industry is based on several interrelated concepts, but the basic one is the Probability of Detection (POD). The POD gives an idea of the probability that a defect is positively detected, given a specimen, a defect size and some noise and system uncertainty conditions. The aim of the following section is to provide an estimation of this probability as a function of such variables.

The detection and characterization of defects is based on the interpretation of the alterations of the measurements due to the presence of the defect. Other model uncertainties and system noises also alter these measurements. We can estimate the POD by the probability that the alteration of the measurement caused by the defect is larger than that caused by the noise. If we label the alteration on the measurement readings caused by the defect as the SIGNAL component, and the alteration generated by the noise as NOISE, the former definition can be formulated as (see Rus *et al.* [29]),

$$POD = P\left(\frac{|\text{SIGNAL}|^2}{|\text{NOISE}|^2} > 1\right) \tag{23}$$

Signal and noise components

The measurement ψ depends linearly on the location and extent of the defects p and the level of noise σ, see Rus *et al.* [30]. Furthermore, three variables are be considered in the problem of maximizing the probability of detection (POD), the level of noise, denoted by σ, the location and extent of the defects, denoted by $\mathbf{p}$, and the cost functional that collects the effects of those in a scalar function f, as defined above. The local damage $\mathbf{p}$ is defined by a five parameters vector, respectively, adimensional centering ordinate, adimensional centering abscissa, damage area, maximum damage level, and form factor.

From the definition of the simulated noise, the dependency of the variation of the measurement with increasing noise is also linear. These two considerations about linearity support the proposal that the measurements on a specimen with noise and

with defect can be expressed as *Taylor series expansion* centered at the case without noise and without defect, and neglecting higher order terms (*hot*) than linear,

$$\psi_i(p,\sigma) = \psi_i(0,0) + \underbrace{p\frac{\partial \psi_i}{\partial p}(0,0)}_{\text{SIGNAL}} + \underbrace{\sigma\frac{\partial \psi_i}{\partial \sigma}(0,0)}_{\text{NOISE}} + hot \tag{24}$$

where $i = 1, ..., N_i$ are the measuring points. The first term on the right hand side is the measurement at point i without noise nor defect. The second term is the alteration of that measurement due to the presence of the defect only, and is labeled SIGNAL, following the reasoning above. The third term is the alteration of the signal originated by the noise only (NOISE).

Finite differences

The second and third terms of the *Taylor* series in depend on the sensitivity of the measurements on the area and the noise respectively, and can therefore be computed by finite differences,

$$\frac{\partial \psi_i}{\partial p}(p_0,0) = \psi_{i,_p}(p_0,0) = \frac{\psi_i(p_0+\Delta p,0) - \psi_i(p_0-\Delta p,0)}{2\Delta p} \tag{25}$$

$$\frac{\partial \psi_i}{\partial \sigma}(0,0) = \psi_{i,_\sigma}(0,0) = \frac{\psi_i(0,\Delta\sigma) - \psi_i(0,0)}{\Delta\sigma} \tag{26}$$

where $p_0 \to 0$ is a small defect used to guarantee that the FEM captures the perturbations produced at small Δp (since the case $p = 0$ with no defect needs to be computed with a topologically different mesh), in order to compute $\psi_{i,_p}(p_0,0) \approx \psi_{i,_p}(0,0)$. In addition, a central difference scheme, which yields an error of the order $O(\Delta p^2)$, becomes available. Since the noise component is linear by definition, a forward difference scheme is adopted, whose $O(\Delta\sigma)$ error is sufficient.

Some authors [31] propose that the parameters Δp and $\Delta\sigma$ should be two orders of magnitude smaller than the values at which the derivative should be computed. However, an estimation of these parameters is studied. It shows $\psi_{i,_p}(0,0)$ and $\psi_{i,_\sigma}(0,0)$ versus Δp and $\Delta\sigma$, respectively, for a defect at the center of the bridge deck. $\Delta p = \Delta\sigma = 10^{-2}$ is shown to produce a stable value of the derivative for the case of the single measurement represented, but the same result is obtained for all 18 measuring points.

On the other hand, (26) yields by direct derivation the last term of the *Taylor* expansion,

$$\frac{\partial \psi_i}{\partial \sigma} = \xi_i RMS(\psi_i^{FEM}) = \xi_i RMS \tag{27}$$

Analytical estimation of the POD

Equations (24), (27) and the relationship $|Y_i|^2 = \frac{1}{m}\sum_{i=1}^{m} Y_i^2$, can be combined into (23) to obtain,

$$\text{POD=P}\left(\frac{p^2 \frac{1}{N_i}\sum_{i=1}^{N_i}(\psi_{i,p}(0,0))^2}{\sigma^2 RMS^2 \frac{1}{N_i}\sum_{i=1}^{N_i}\xi_i^2} > 1\right) = \text{P}\left(p^2 > \frac{RMS^2\sigma^2\sum_{i=1}^{N_i}\xi_i^2}{\underbrace{\sum_{i=1}^{N_i}(\psi_{i,p}(0,0))^2}_{S_p}}\right) \tag{28}$$

If the noise generator ξ_i is a random variable, the POD is a probability of the stochastic variable p^2, described by the cumulative probability density function F,

$$POD = F\left(\frac{RMS^2\sigma^2\sum_{i=1}^{N_i}\xi_i^2}{S_p}\right) \tag{29}$$

Using Monte Carlo techniques and error propagation theory the noise in the measurement points can be concluded to follow a normal distribution. Assuming this distribution, the squared sum of the noise ξ_i is known to follow a *Chi-square* distribution, since $\sum_{i=1}^{N_i}\xi_i^2 \longrightarrow \chi^2_{N_i}$ (e.g. [26]). The parameter of the *Chi-square* distribution is the number of degrees of freedom N_i, which in this case is the number of measurement points. In the case that $N_i > 10$, the *Chi-square* distribution can be approximated by a Gaussian or normal N distribution $\chi^2(N_i) \approx N(N_i - 2/3, \sqrt{2N_i})$ with mean $N_i - 2/3$ and standard deviation $\sqrt{2N_i}$. This approximation in (29) yields,

$$p^2 \longrightarrow N\left[\frac{RMS^2\sigma^2(N_i - 2/3)}{S_p}, \frac{RMS^2\sigma^2\sqrt{2N_i}}{S_p}\right] \tag{30}$$

Since $F(x) = \int_{-\infty}^{x} f(y)dy$ is the cumulative of the normal probability density function f, whose inverse is $x = G(F(x))$, the useful defect area to noise ratio p/σ can be expressed from (30) given a POD level as,

$$\frac{p}{\sigma} = \sqrt{\frac{RMS^2(N_i - 2/3)}{S_p}\left(1 + G[POD]\frac{\sqrt{2N_i}}{N_i - 2/3}\right)} \tag{31}$$

Note that the analytical expression (30) is only valid for noise with normal distribution at the measurement points.

4. Numerical result

4.1. Forward problem

A bridge deck with dimensions 8×20 m and thickness 0.5 m is tested. The boundary conditions are simple support on two opposite sides. Figure 3 shows the simulated search results, experiment and non damage measurement by FEM without noise. An moving load is applied at the red marked point with speed 40 km/h along the middle of the bridge, and measurements are made at the 18 points distributed over a regular 3×6 mesh, see Figure 2.

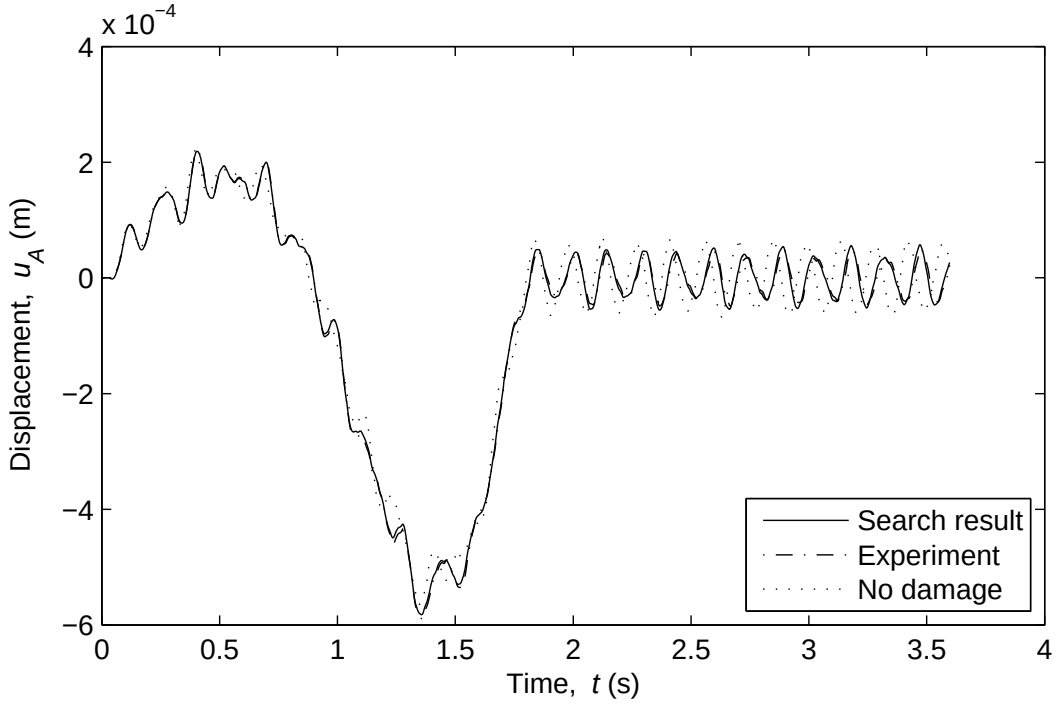

Figure 3. Measurements without noise.

4.2. Search convergence

The moving load has a magnitude of 10000 kg, whereas the measurement recording period is 3 ms. Figure 4 shows the calibration results without noise, predictive damage

distribution (white) againt the real damage distribution (gray). Predictive damage distribution converges with high accuracy, it verify the predictive model.

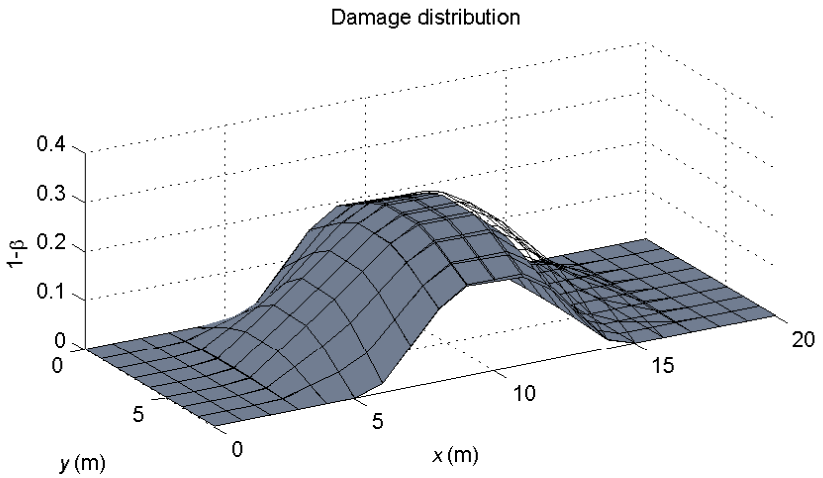

Figure 4. Damage model results without noise.

In this section, the search algorithm is studied, adjusting the GA parameters to archieve a computational effiency and to guarantee a good convergence for zero noise.

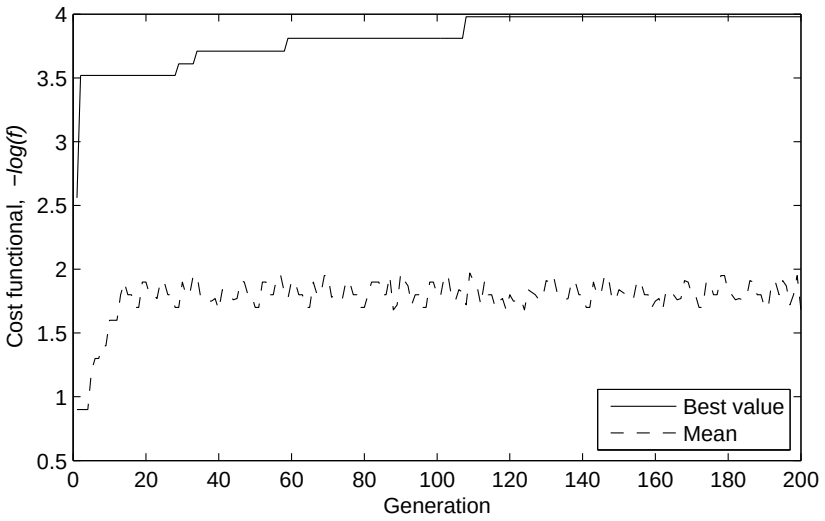

Figure 5. Evolution of the GA in the case without noise, for 50 individuals and 200 generations.

The Figure 5 plots the evolution of the population mean versus each generation. To ensure that the solution does not converge to a local minimum, genetic diversity was injected by mutation and crossover parameters. To guarantee the convergence to a global optimum, while establishing a compromise between IP error and computational cost, the GA selected parameters are shows in Table 1.

Parameter	Value
Population size	50
Number of generations	200
Probability of crossover	0.80
Probability of mutation	0.30
Probability of selection	0.70

Table 1. Parameters used for the GA search algorithm.

The choice of these values was made based on a test in which it has found a successful values with a good computational cost. Figure 6 and 7 shows the evolution of the cost function for several values of population and genetarion. The improvement achieved by increasing above the established values of population and generations is never significant.

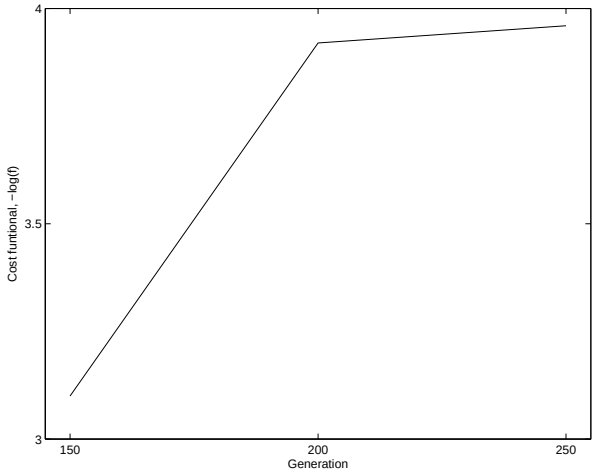

Figure 6. Cost function evolution with generations.

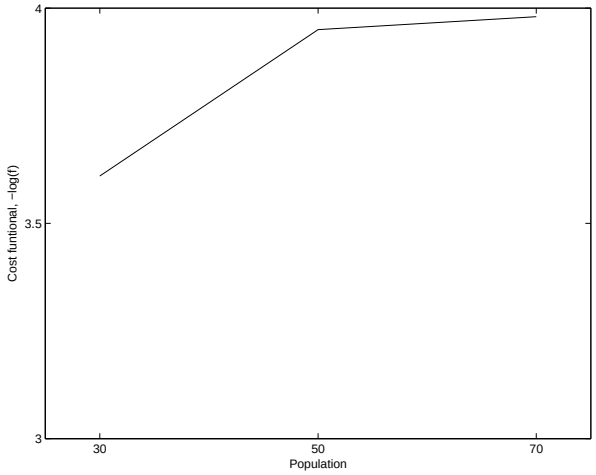

Figure 7. Cost function evolution with population.

Figure 8 shows the predictive damage distribution againt the real damage distribution and it can see the genetic algorithm evolution, optimum is reached for 122 generations. Predictive damage distribution converges with high accuracy for noise level 0.1 %.

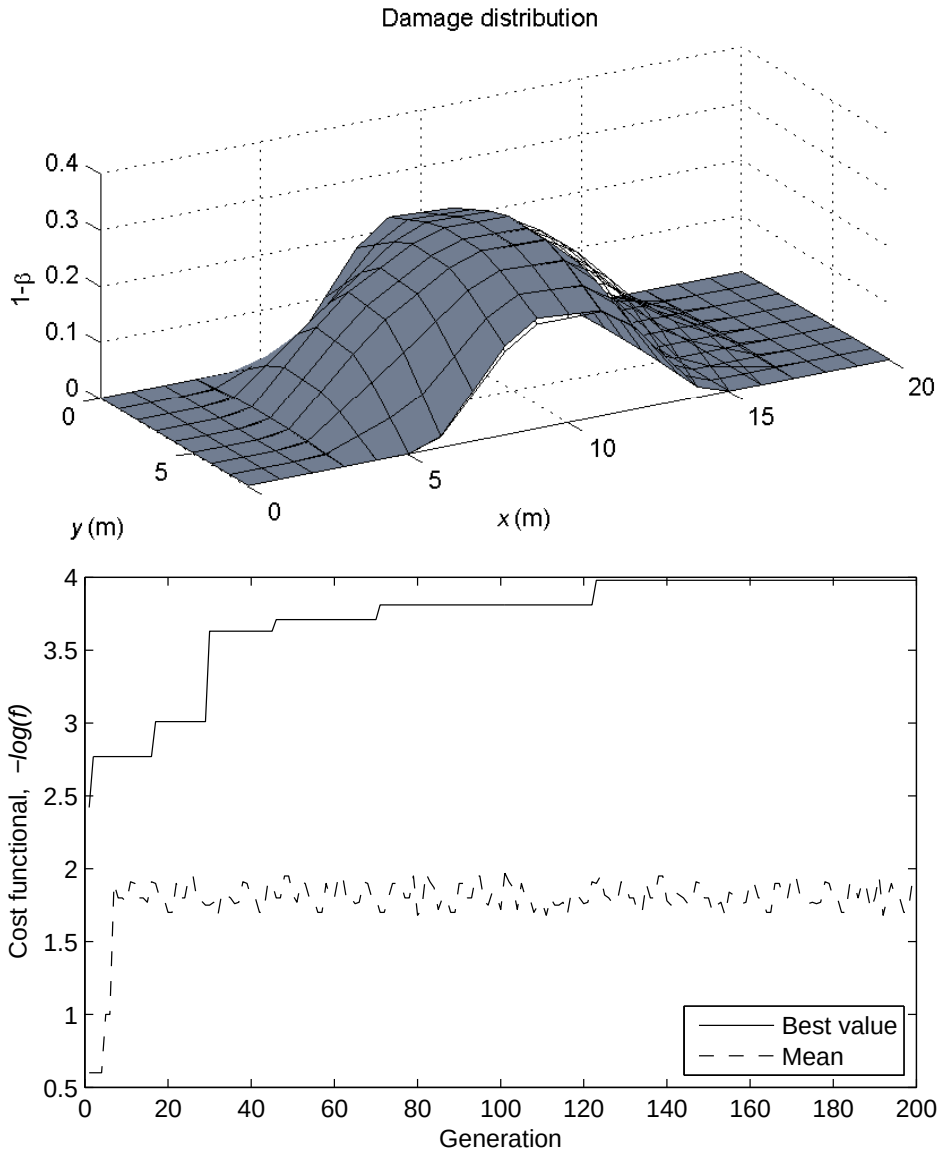

Figure 8. Damage model resultsand evolution of the GA for noise 0.1 %.

Figure 9 shows predictive damage distribution converges with high accuracy for noise level 0.3 %. In Figure 9 below, the optimum cost function is reached for 105 generations.

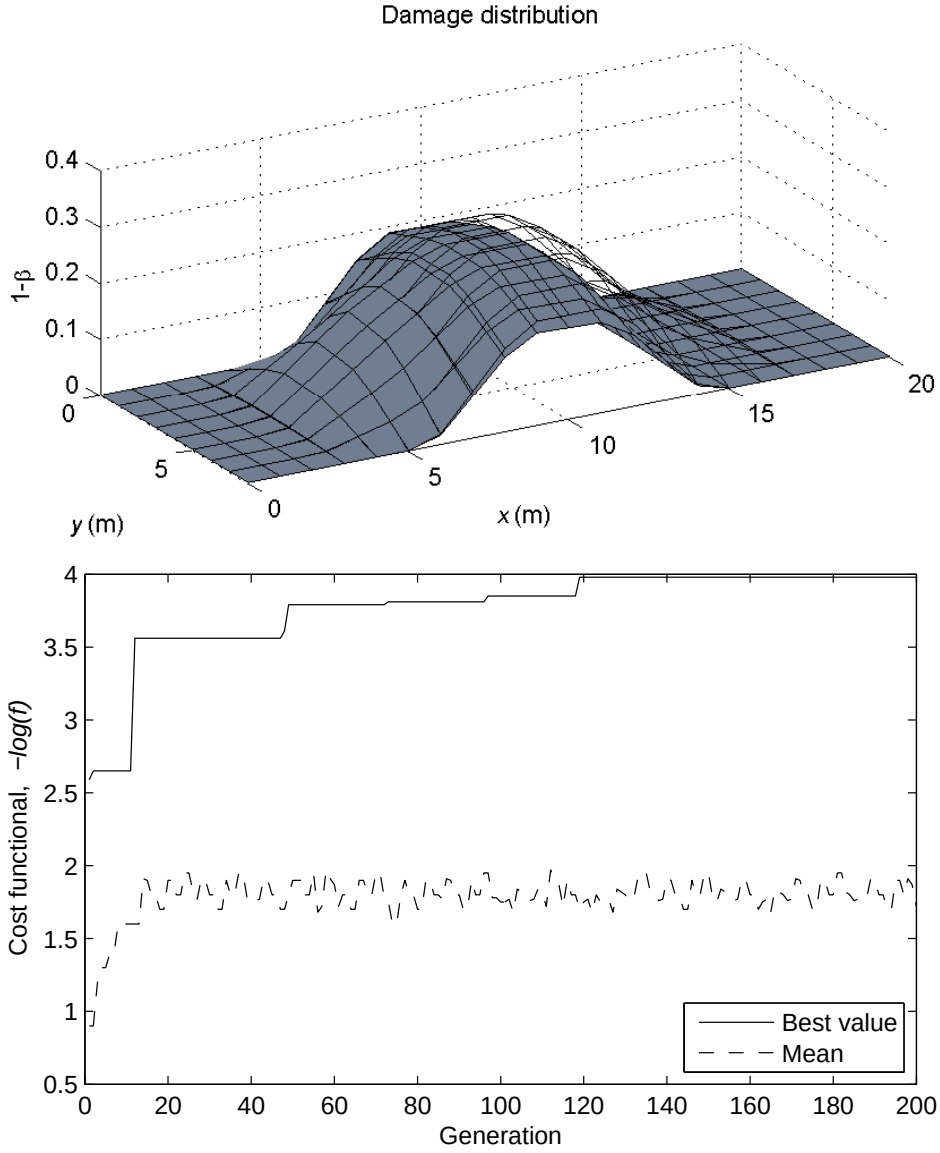

Figure 9. Damage model results and evolution of the GA for noise 0.3 %.

Figure 10 shows predictive damage distribution converges with accuracy for noise level 1 %. In Figure 10 below, the optimum cost function is reached for 140 generations. The number of generations have grown by almost 35 points and have lower precision in search results, but not significantly.

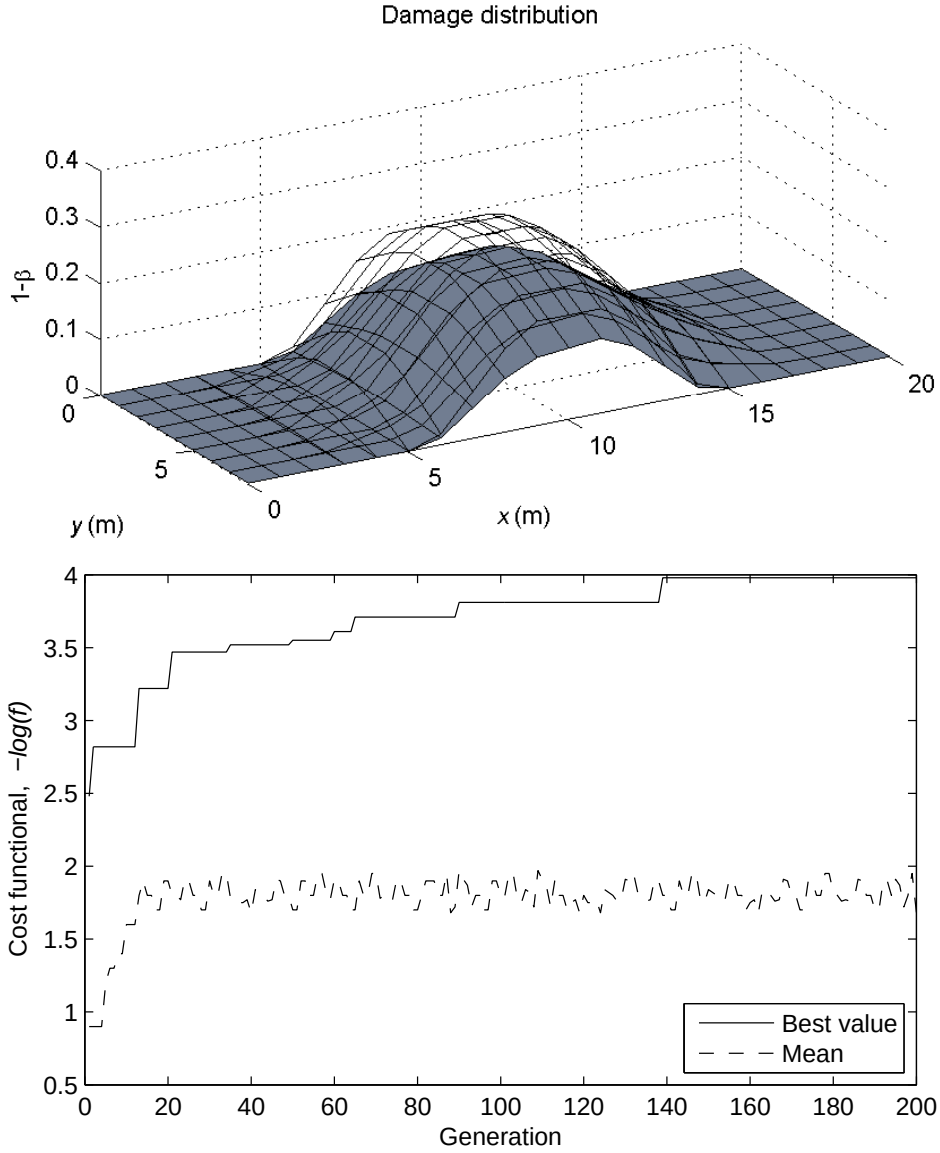

Figure 10. Damage model results, measurement and evolution of the GA for noise 1.0 %.

Figure 11 shows predictive damage distribution converges with medium accuracy for noise level 3 %. In Figure 11 below, the optimum cost function is reached for 160 generations. The number of generations have grown by almost 20 points and have lower precision in search results.

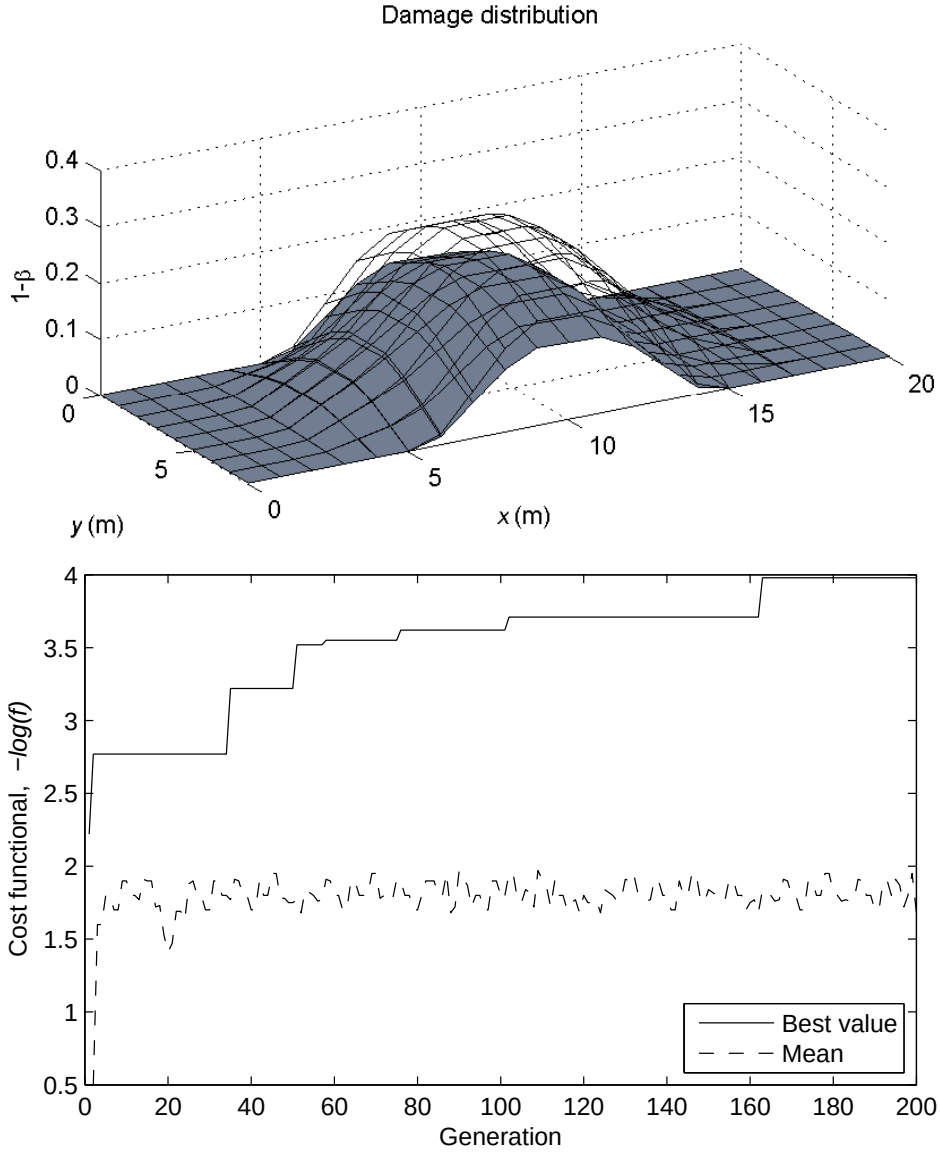

Figure 11. Damage model results, measurement and evolution of the GA for noise 3.0 %.

Figure 12 and 13 above shows predictive damage distribution doesn't converges for noise level 10 % and 20 %. This is verified by Figure 19 and Figure 20, because the POD is not enough to ensure the search for any level of damage. Similarly, Figure **??** checks that the distance of damage exceeds the unit for these noise levels.

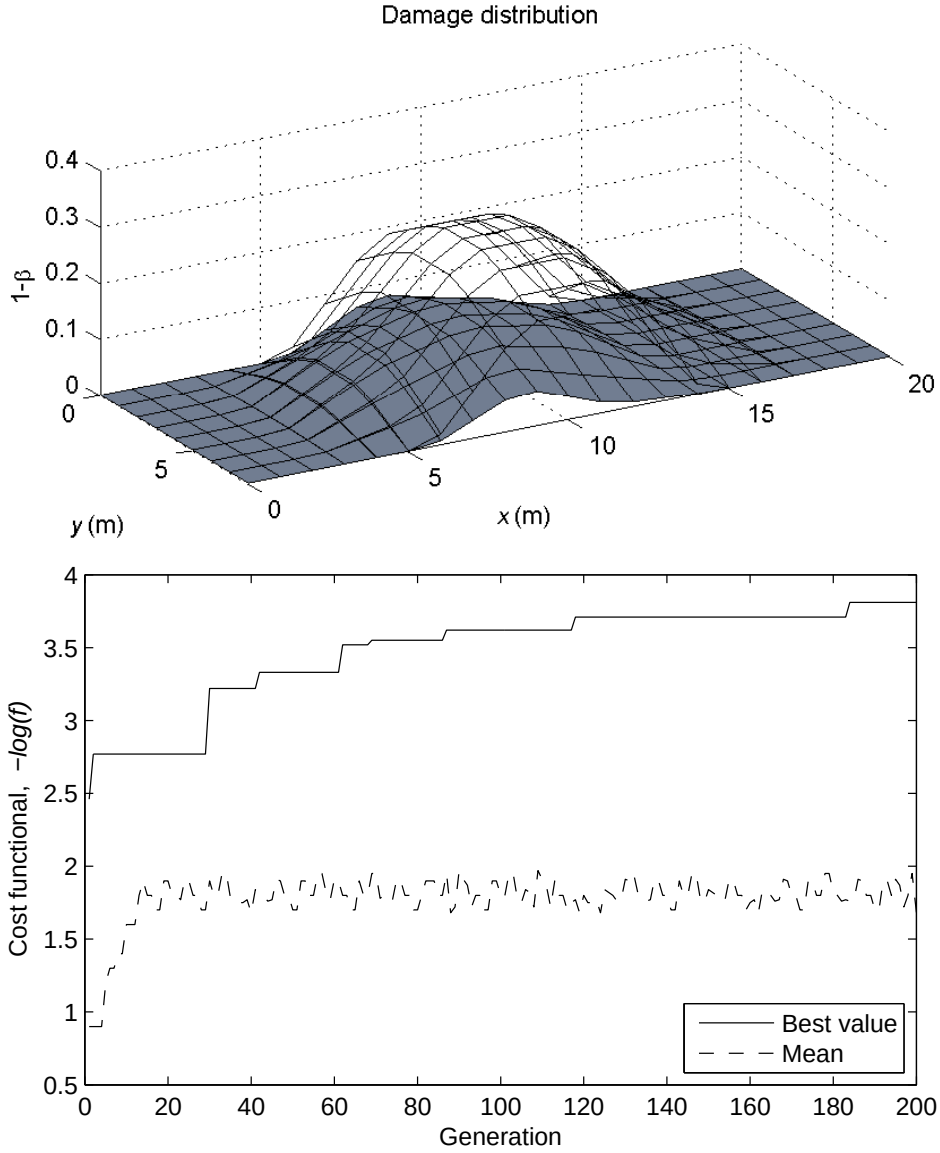

Figure 12. Damage model results, measurement and evolution of the GA for noise 10 %.

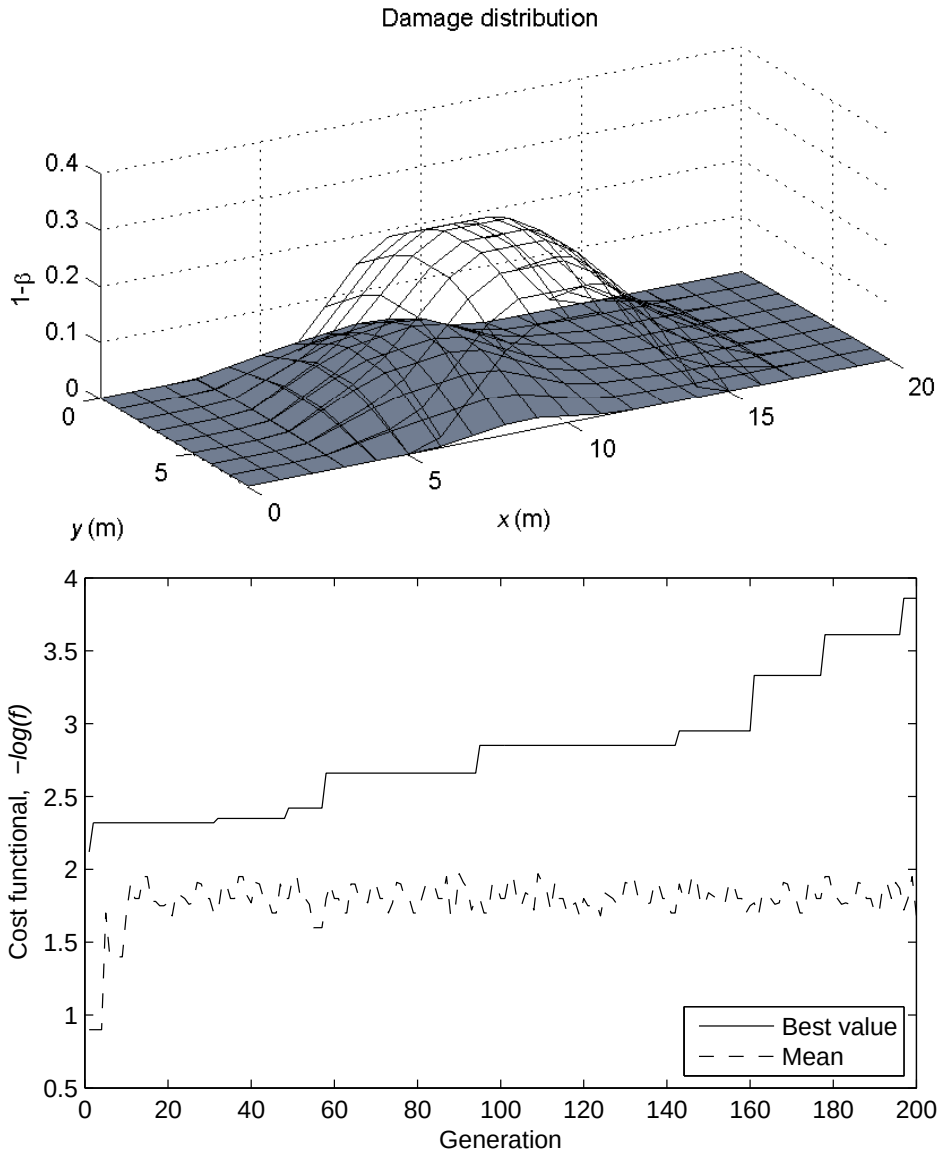

Figure 13. Damage model results, measurement and evolution of the GA for noise 30 %.

4.3. Filtered optimum

Now, a standard GA is implemented for the search of the defect and the optimal filter. This is done first by considering the time windowing, the selction of measurement points and the wavelet levels. The characteristic parameters for tuning the GA are a crossover fraction of 0.6 and a mutation fraction of 0.4. The number of generation is 200, and the number of individuals in the population is 50. For the optimization of the POD, the term p/σ is aproximated by finite diferences using $\epsilon_p = 0.01$ and $\epsilon_n = 0.01$. These values fall empirically within a wide range of finite difference steps that does not affect

significantly the final value. Figure 14 shows the probability of detection without noise for different filters and without. We can see that the improvement made by the filters is not representative, since the noise level is negligible.

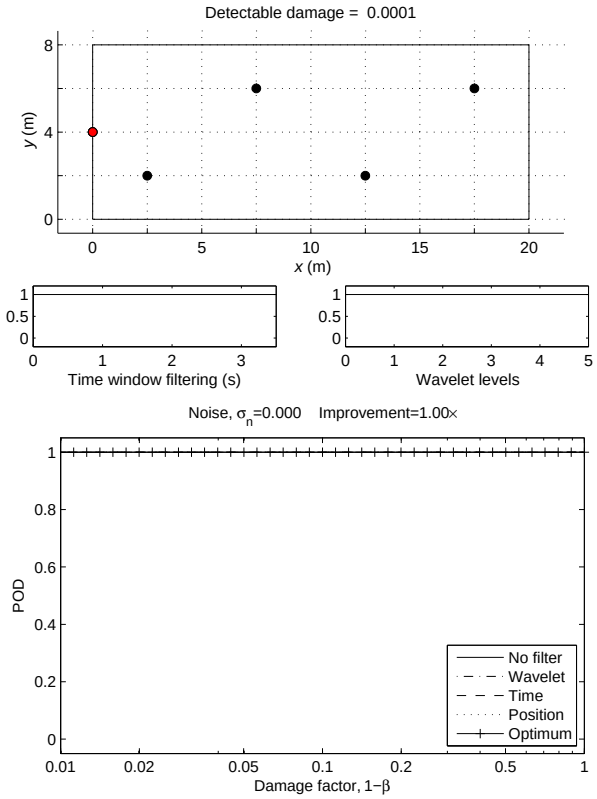

Figure 14. Probability of detection with and without filtering, optimization of the measurement point filter, time window filter and wavelet filter.

The wavelet level and time windows optimization is performed with the minimum possible number of bits to represent the combination of measurement point, 5 bits for the five wavelet levels and 5 bits for the five reference points in time. An example of this is given in Figure 14, where the minimum damage that can be found is 0.0001, and inversely proportional to the allowed noise level Figures 15, 16, 17, 18, 19 and 20.

In Figure 21 is showed, in order to perform the convergence analysis, the distance between the parameters that characterize the real and the calculated defects are defined by the norm defined by Equation 32.

$$d = \frac{\sqrt{\sum_{i=1}^{N} \left(\tilde{p}_i - p_i^c\right)^2}}{\sum_{i=1}^{N} \tilde{p}_i} \tag{32}$$

Figure 15 shows the POD for several level of damage and it shows filters influence is not very representative, with a improvement of 0.82. We can see the filters influence begins to be noticeable but still not very representative, with a improvement of 0.82. The wavelet and time windowing filters are optimized reaching all frequencies, see Figure 15. The damage detectable is 0.0421.

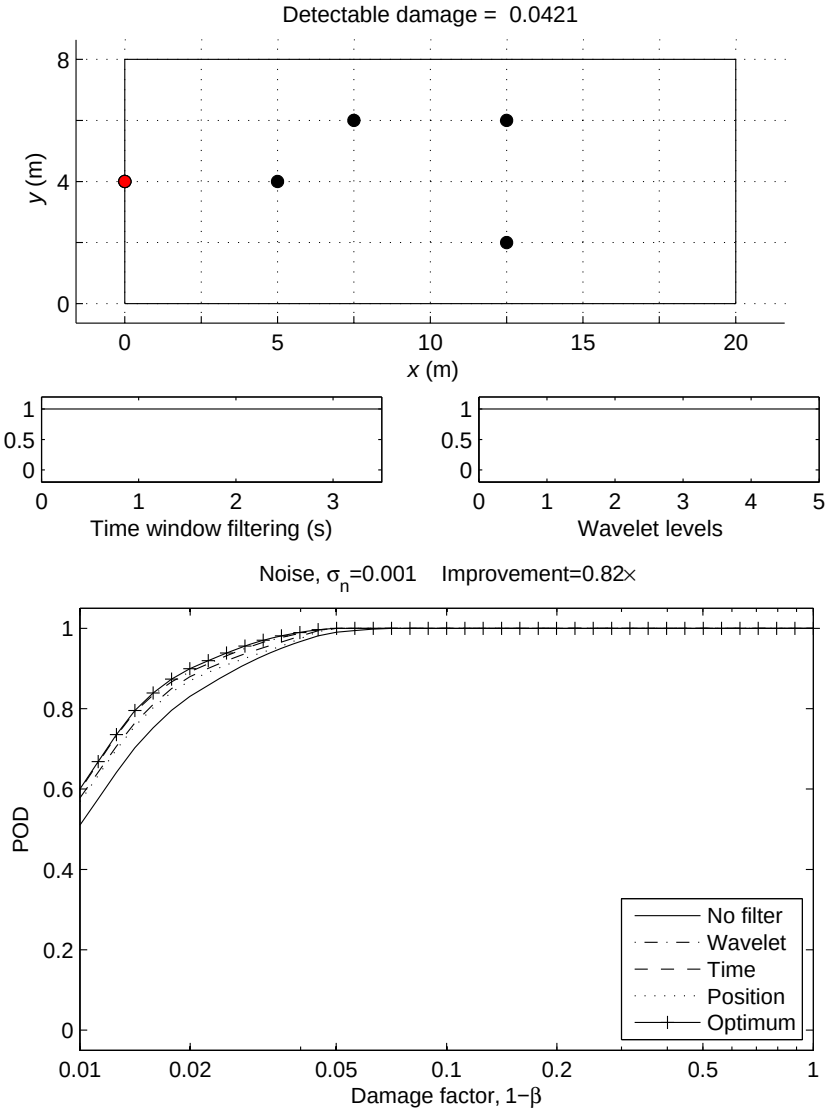

Figure 15. Probability of detection with and without filtering and sequential optimization of the measurement point filter, time window filter and wavelet filter for noise 0.1 %.

The wavelet and time windowing filters are optimized reaching all frequencies, see Figure 16. The damage detectable is 0.0492.

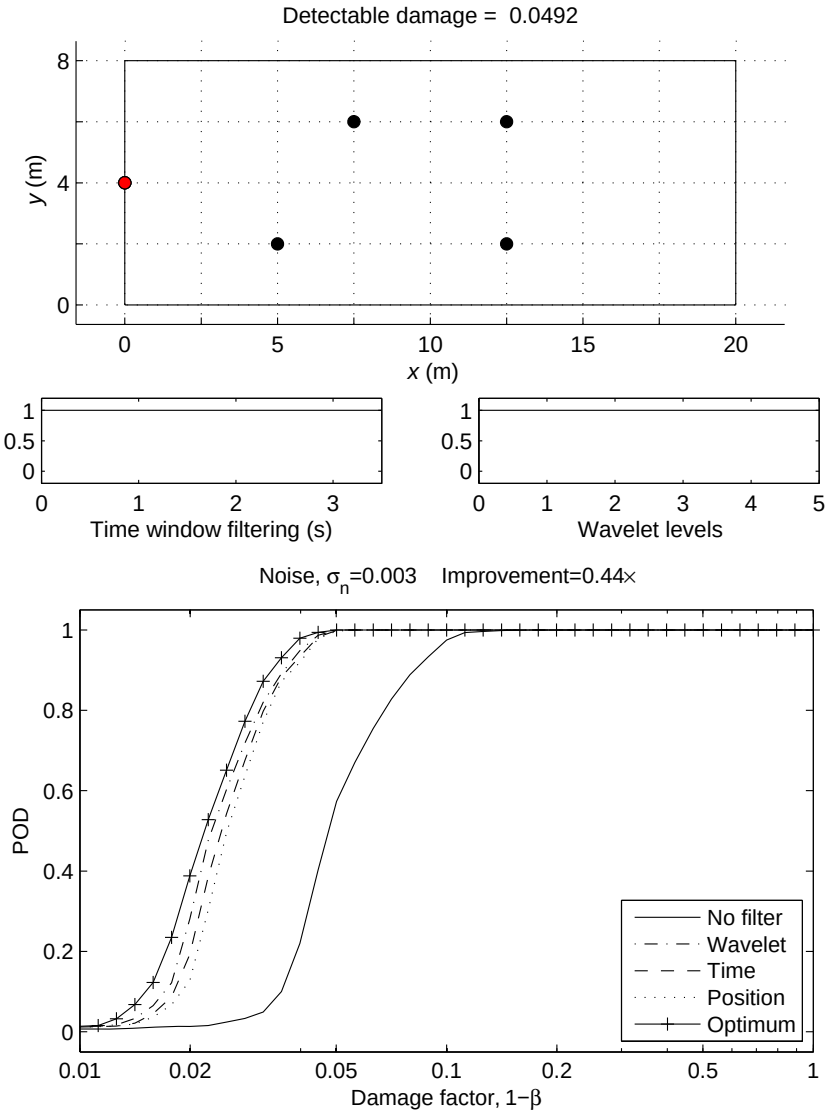

Figure 16. Probability of detection with and without filtering and sequential optimization of the measurement point filter, time window filter and wavelet filter for noise 0.3 %.

Figure 17 shows the filters influence is very representative, with a improvement of 0.25. The wavelet and time windowing filters aren't optimized reaching high frequencies, see Figure 17 below. The damage detectable is 0.1920.

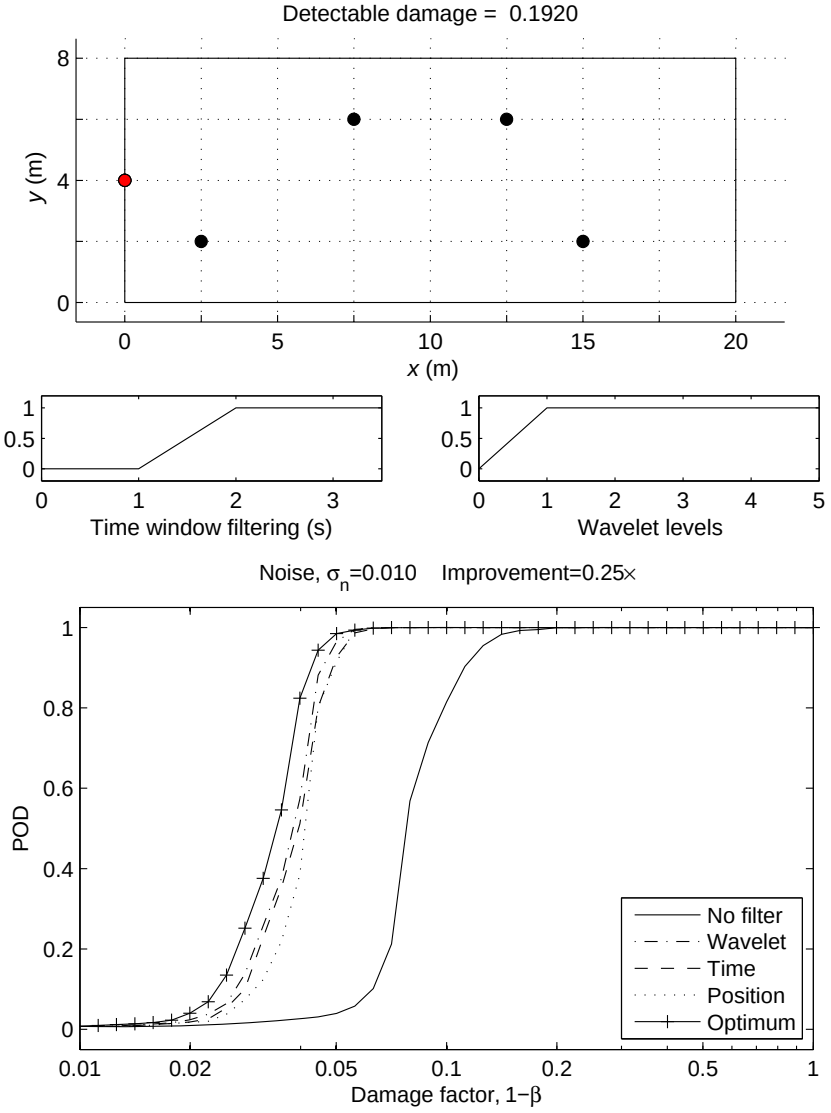

Figure 17. Probability of detection with and without filtering and sequential optimization of the measurement point filter, time window filter and wavelet filter for noise 1.0 %.

Figure 18 shows the filters influence is very representative, with a improvement of 0.25. The wavelet and time windowing filters aren't optimized reaching high frequencies, see Figure 18 below. The damage detectable is 0.1917.

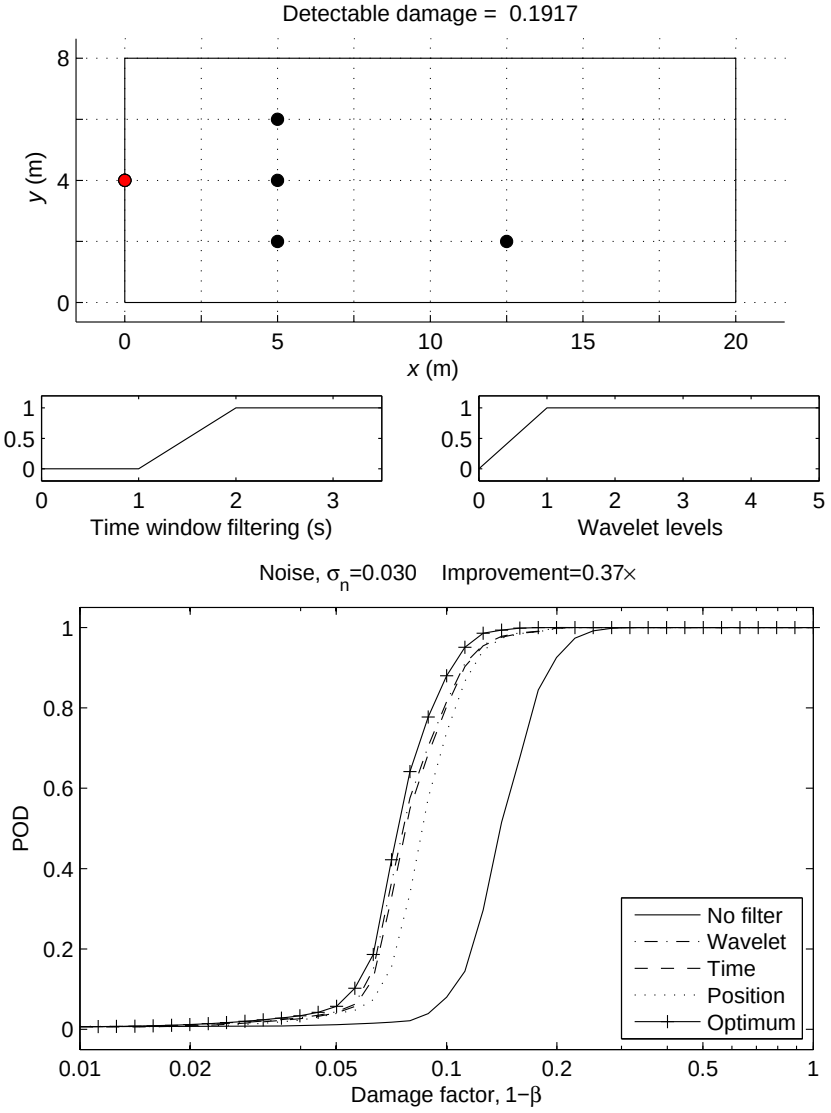

Figure 18. Probability of detection with and without filtering and sequential optimization of the measurement point filter, time window filter and wavelet filter for noise 3.0 %.

Figure 19 and Figure 20 shows that filtering is not sufficient to achieve improved results. For noise levels above 10 % failed to detect any level of damage implemented the optimal filter.

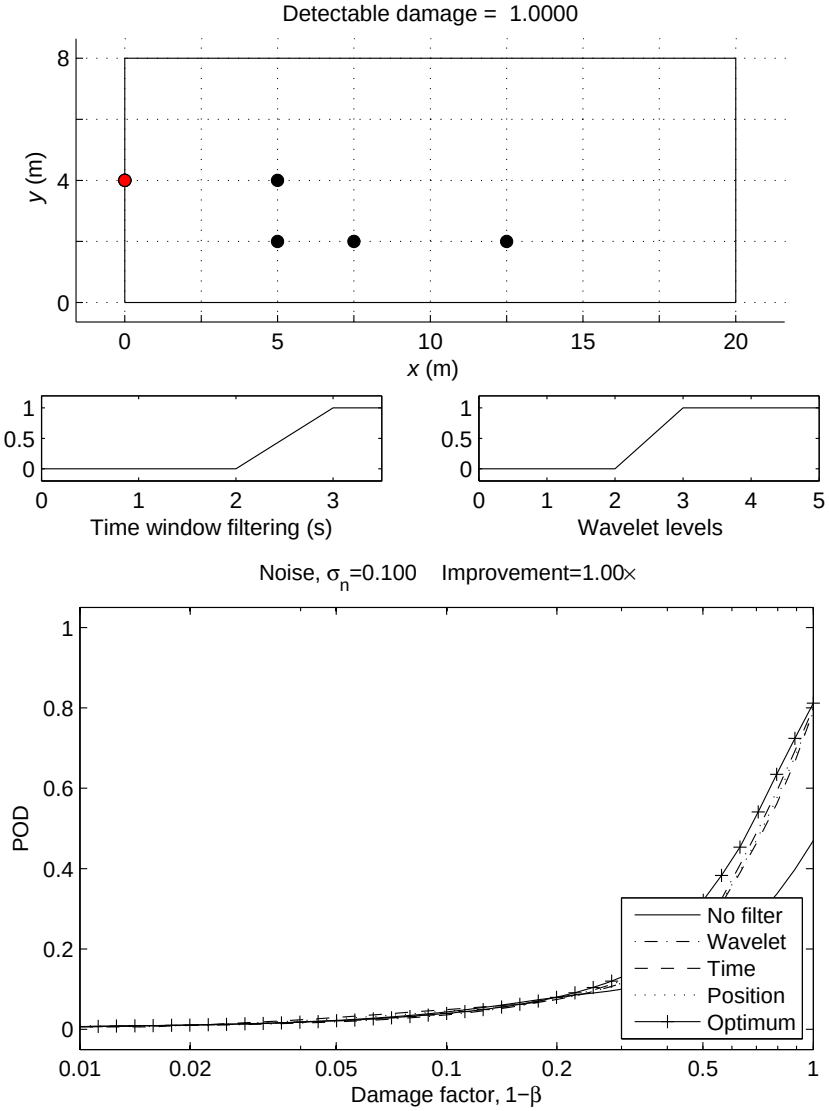

Figure 19. Probability of detection with and without filtering and sequential optimization of the measurement point filter, time window filter and wavelet filter for noise 10 %.

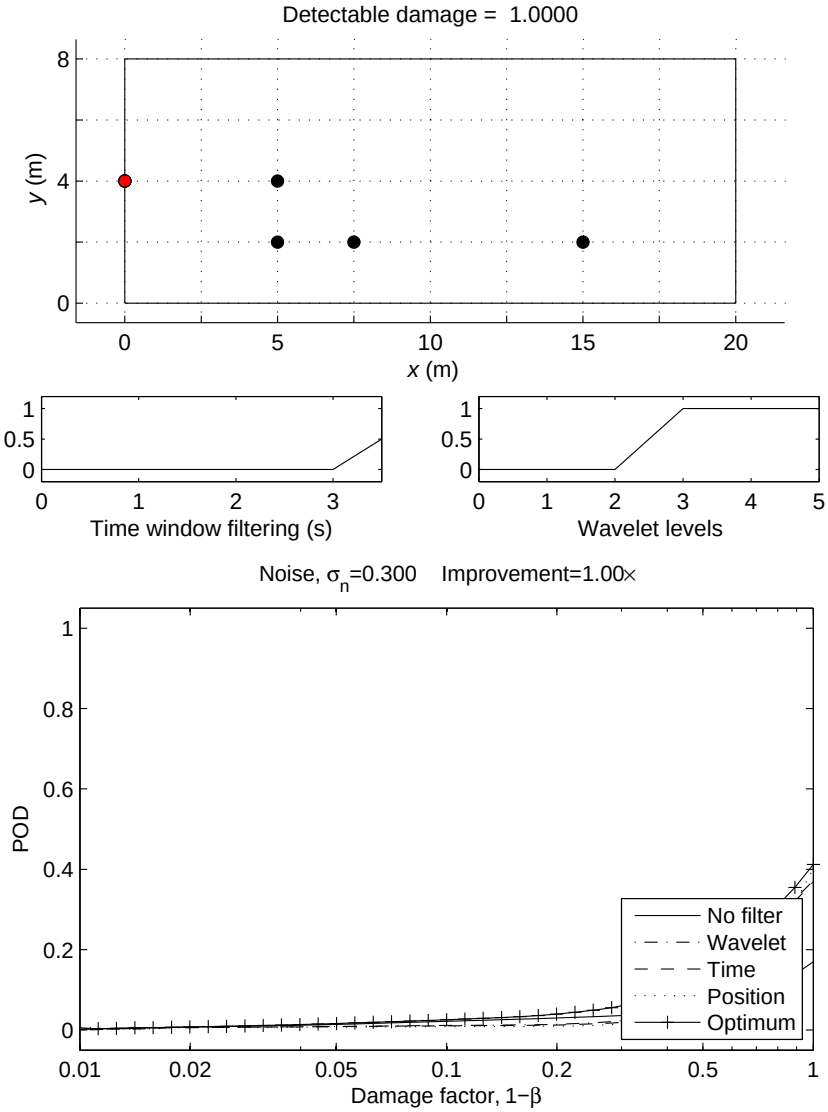

Figure 20. Probability of detection with and without filtering and sequential optimization of the measurement point filter, time window filter and wavelet filter for noise 30 %.

4.4. Noise effect

Figure 21 plots the distance, see Equation 32, between real and reconstructed damage parameters, versus system noise levels. The results showed on the particular local damage parametrization, for a 8 x 20 m bridge dimensions with thickness 0.5 m, and speed 40 km/h. Figure 21 shows good results up to 3 % of noise.

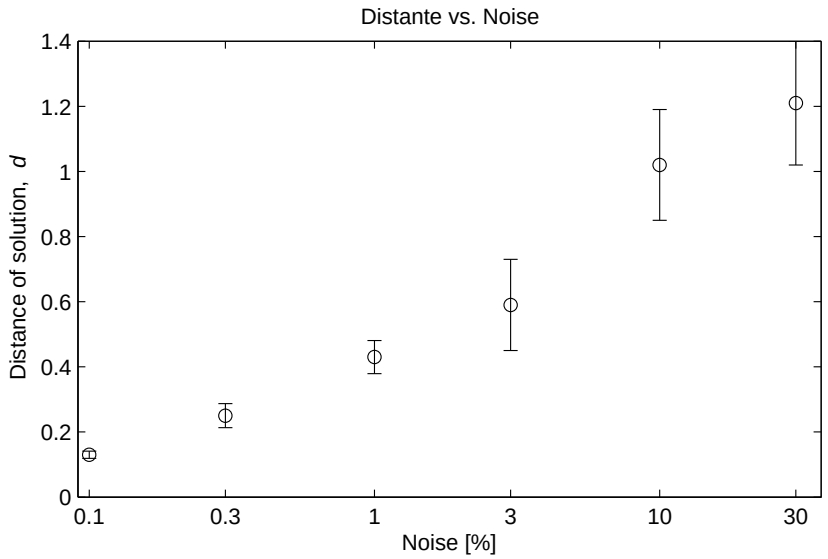

Figure 21. Distance of damage as a function of the noise in measurements.

4.5. POD validation

Three cases presented previously we used to validate and robustness of the formulation of the POD, it observed a linkage between results that exceed the distance of the damage the unit and did not reach a detection probability for any level of damage, see the relation, Figure 22. This relationship holds in the parametric study presented below. For example, to a noise level of 3 % level of damage for which the POD reaches = 50 % is 0.148 and the distance is 0.42, both results show a direct relationship, and the noise level for which the distance of damage is greater than 0.5 is 3.97 %, logically just over 3%.

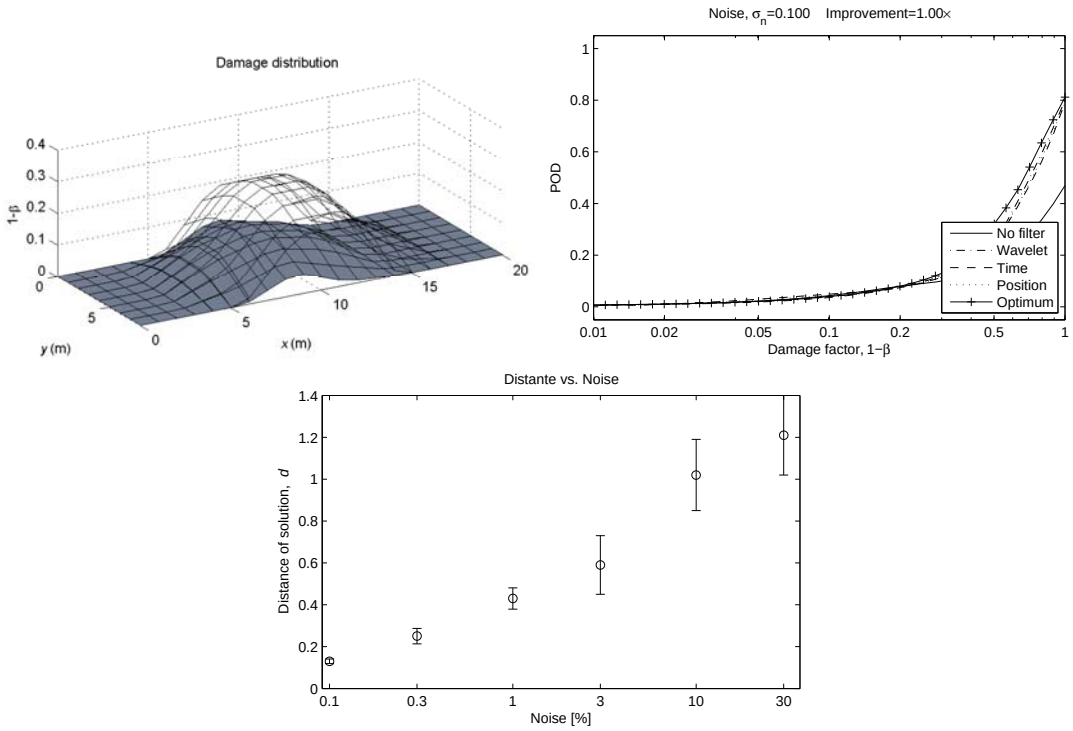

Figure 22. POD validation.

4.6. Parametric study

Figures 23, 26 and 27 plot the distance, see Equation 32, between real and reconstructed damage parameters, versus system noise levels. The results showed on the particular local damage parametrization, for a 8 x 20 m bridge dimensions with thickness 0.5 m and speed 40 km/h in Figure 21 is studied for different cases of lengths and thicknesses of the bridge, and different speeds, to verify the consistency of the method. The distance unit is a dispersion of results of 100 %. Figures 24, 25 and 28 plot the POD for each case, noticeable a direct relationship between all results.

With increasing length of the bridge there is a greater sensitivity to noise to obtain worse results, see Figure 23. For a length of 80 m, it reaches a given distance, or drive. Figure 24 shows how da pod, or detected with POD unit is reduced with increasing the length of the bridge, until it stops 80 m does not reach the POD unit.

Figure 26 shows that for thickness between 0.5 and 0.7 m achieved good results up to 3 % of noise, but for a thickness of 0.3 is reduced to 1 %. Figure 24 shows how the POD, value less unit does for noise 3 % and thickness noise 0.3 m.

Figure 27 shows between 20 and 120 km/h, speed limits on roads, not cause a trend in the results, staying around the same values. This is verified in Figure 28.

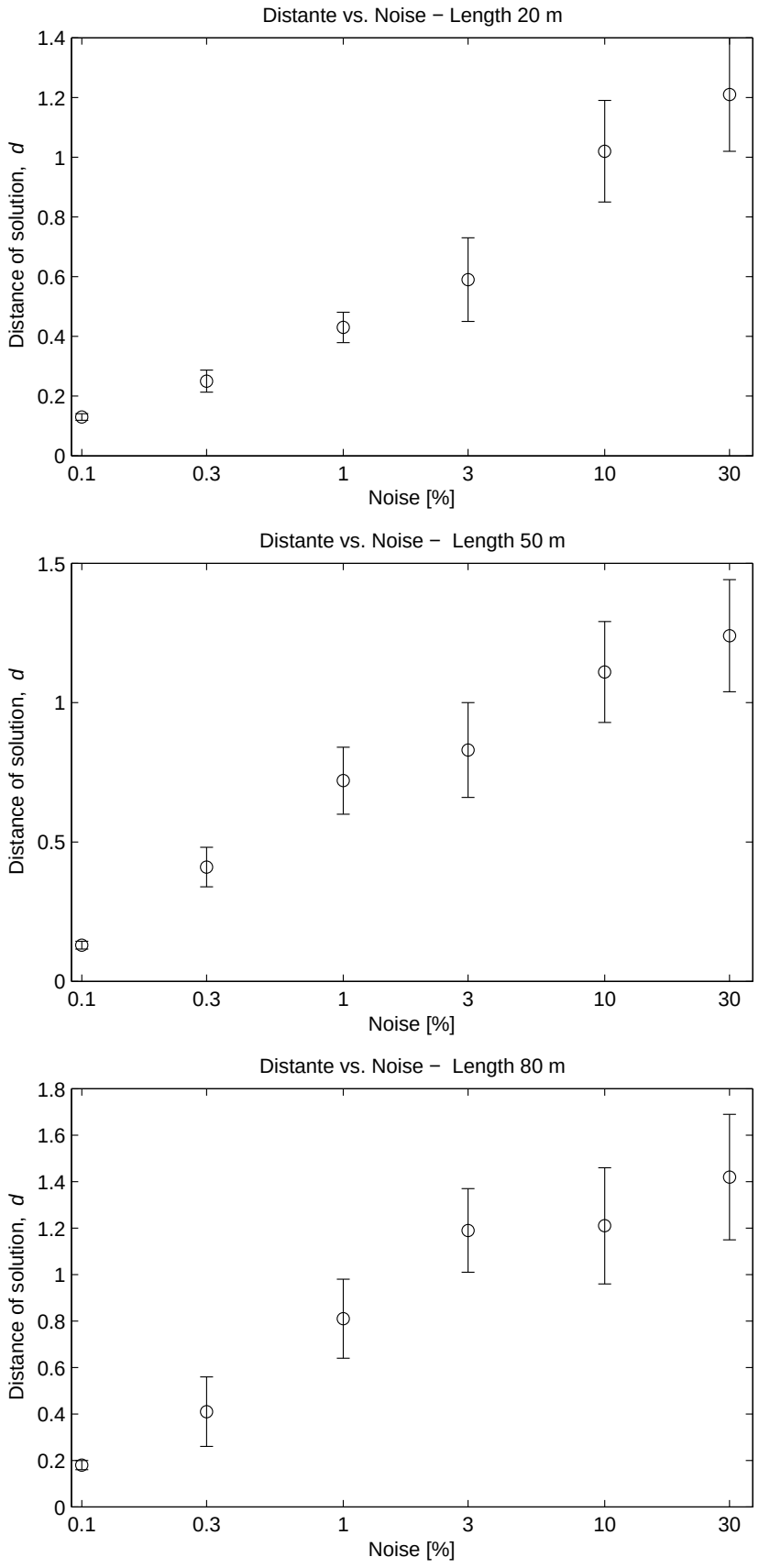

Figure 23. Distance of the damage as a function of the noise in measurements, for several lengths.

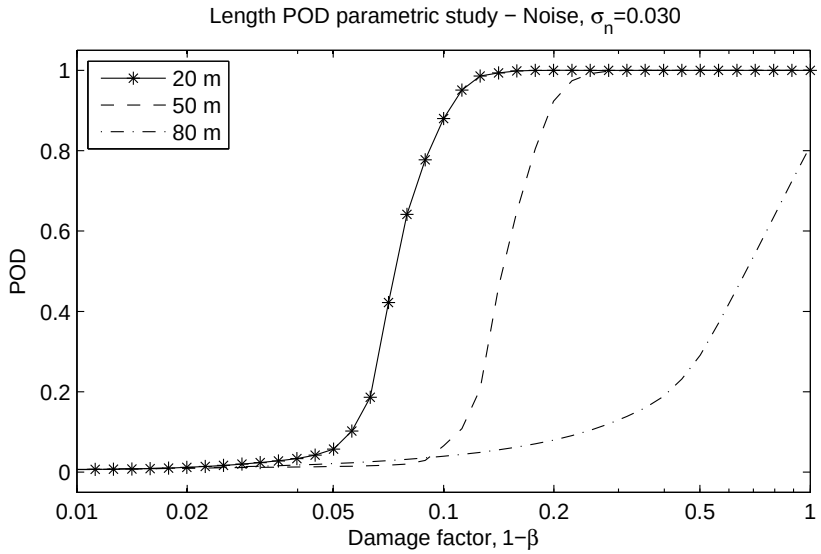

Figure 24. Probability of detection, for several speeds and noise 3%.

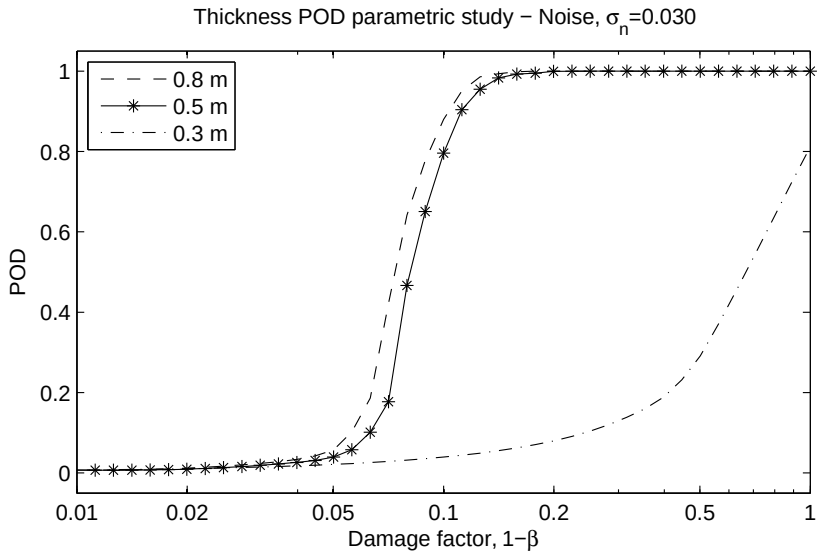

Figure 25. Probability of detection, for several thickness and noise 3%

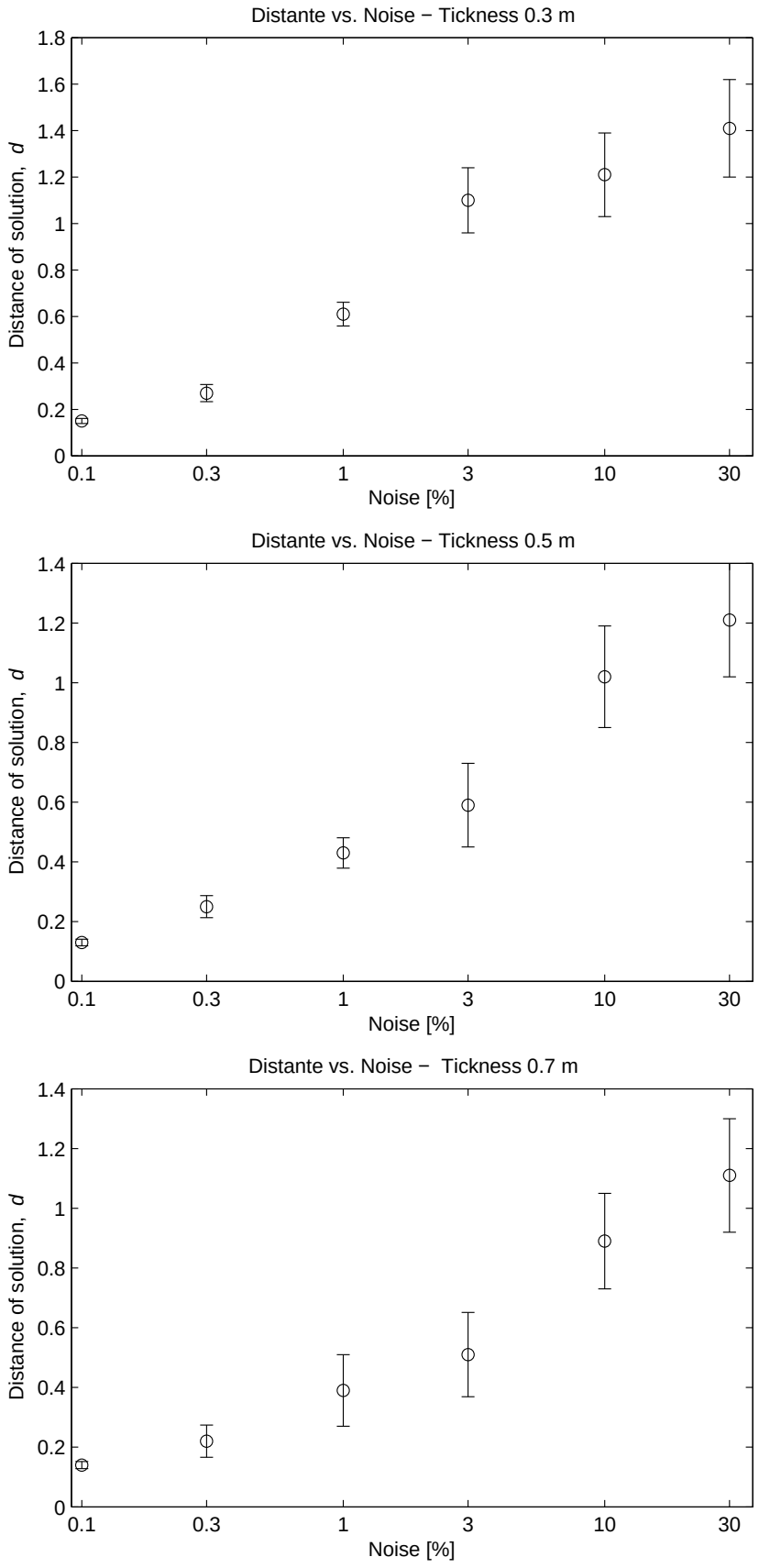

Figure 26. Distance of the damage as a function of the noise in measurements, for several tickness.

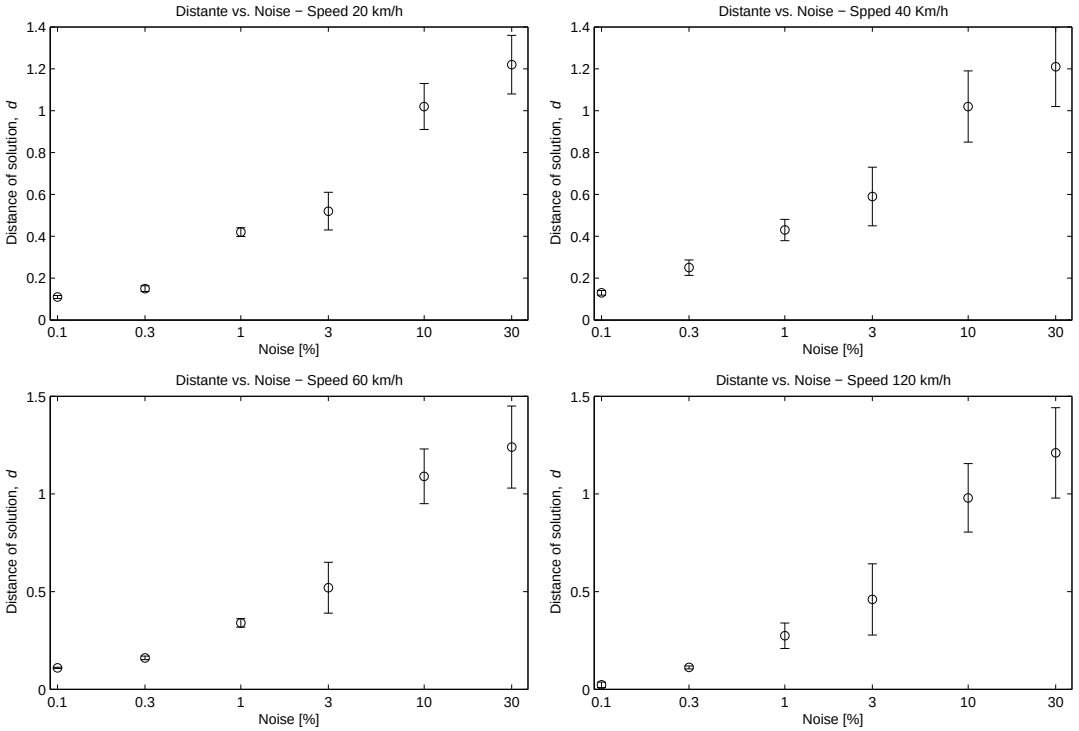

Figure 27. Distance of the damage as a function of the noise in measurements, for several speeds.

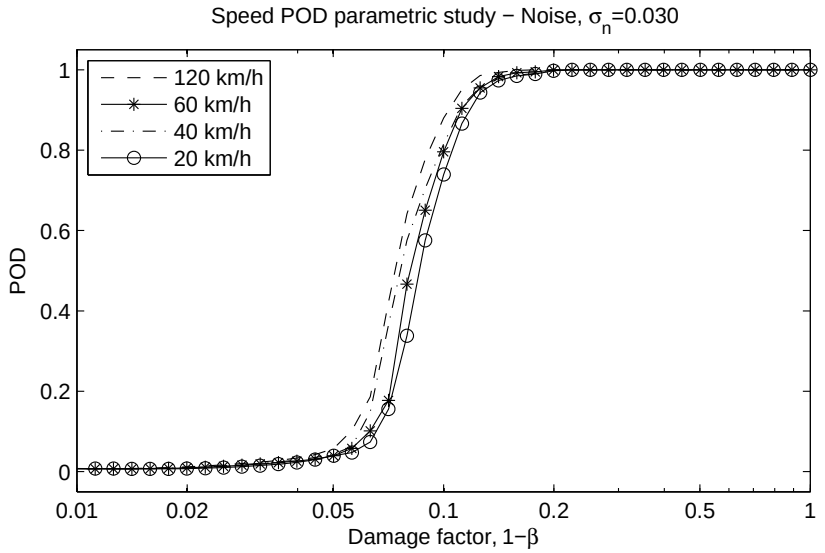

Figure 28. Probability of detection, for several speeds and noise 3%.

5. Conclusions

An inverse problem strategy is defined and tested in this work, which is capable of identifying and characterizing a degree of degradation defect in plate bridge decks when noise in the measurements are present. To quantity the level that a defect is positively detected, given a specimen, an analitycal formulation of Probability of Detection is defined, function of the location and extent of the defects, the level of noise and the cost function. A new damage model that makes it possible to parameterize the damage more trustworthy is defined. A parametric study is performed to within range of values that the method produced good results. The POD's formulation is validated for the cases presented, its relevance and robustness in all cases is demonstrated. It is concluded that, by applying the proposed model based inverse problem strategy, it is possible to reconstruct the characteristics of a damage with sufficient precision under realistic levels of noise in measurements. It is concluded from this study that the approach works well for the numerical tests, especially for complex structures such as bridge deck plates under moving loads. Even under the consideration of noisy effects in the measurements, the proposed method is useful for reconstructing the stiffness degration damage. However, in order to prove the effectiveness of the technique for real-life situations, it will be necessary to prove the concept from experimental studies and adapting the continuum damage model to observations.

Acknowledgements

The author wourld like to thank the Consejería de Economía, Innovación y Ciencia, Junta de Andalucía, Spain, for the FPU grant 760503. Author would also like to thank Prof. Guillermo Rus for his invaluable contributions to the development of the present work.

References

[1] P. Addison, The little wave with the big future. Physics World, March 2004, 3539.

[2] F. T. K. Au, Y. S. Cheng, L. G. Tham and Z. Z. Bai, Structural damage detection based on a micro-genetic algorithm using incomplete and noisy modal test data. Journal of Sound and Vibration 259(5) (2003) 10811094.

[3] K. J. Bathe, The finite element procedures in engineering analysis. Prentice Hall, Englewood Cliffs, New Jersey, 1996.

[4] J. H. Chou and J. Ghaboussi, Genetic algorithms in structural damage detection. Computers and Strutures 79 (2001) 13351353, .

[5] M.I. Friswell, J.E.T. Pennyb, and S.D. Garvey, A combined genetic and eigensensitivity algorithmfor the location of damage in structures. Computers and Structures 69 (1998) 547556.

[6] R. Gallego and G. Rus, Identification of cracks and cavities using the topological sensitivity boundary integral equation. Computational Mechanics 33, 2004.

[7] D. Goldberg, Genetic algorithms in search, optimization and machine learning. Addison-Wesley Publishing Co., Reading, Massachusetts, 1989.

[8] S. C. Han, S. Y. Lee and G. Rus, Postbuckling analysis of laminated composite plates subjected to the combination of in-plane shear, compression and lateral loading. International Journal of Solids and Structures, in press, 2005.

[9] K. Il Lee and S. W. Yoon, Comparison of acoustic characteristics predicted by biots theory and the modified biot-attenboroughmodel in cancellous bone. Journal of Biomechanics, 2005.

[10]] A. A. Kideir and J. N. Reddy, Dynamic response of antisymmetric angle-ply laminated plates subjected to arbitrary loading. Journal of Sound and Vibration 126(3) (1988) 437445.

[11] I. K. Kim and Y. Y. Kim, Damage size estimation by the continuous wavelet ridge analysis of dispersive bending waves in a beam. Journal of Sound and Vibration, in press, 2005.

[12] M. Krawczuk, Application of spectral beam finite element with a crack and iterative search technique for damage detection. Finite Elements in Analysis and Design 38 (2002) 537548.

[13] I. Kreja, R. Schmidt and J. N. Reddy, Finite elements based on a first-order shear deformation moderate rotation theory with applications to the analysis of composite structures. International Journal of Non-Linear Mechanics 32(6) (1997) 11231142.

[14] A. Kumar and R. P. Shrivastava, Free vibration of square laminates with delamination around a central cutout using high-strain dynamic testing. Composite Structures 70(3) (2005) 317333.

[15] S. J. Lee, Y. H. Kim and C. S. Song, Diagnosis of mechanical fault signals using continuous hidden markov model. Journal of Sound and Vibration 276 (2004) 10651080, .

[16] S. Y. Lee and S. C. Wooh, Detection of stiffness reductions in laminated composite plates from their dynamic response using themicrogenetic algorithm. Computational Mechanics 36 (2005).

[17] S. Y. Lee and S. C. Wooh, Waveform-based identification of structural damage using the combined fem and microgenetic algorithms. Journal of Structural Engineering, ASCE, 131(9) (2005) 14641472.

[18] S. Y. Lee and S. S. Yhim, Dynamic analysis of composite plates subjected to multi-moving loads based on a third order theory. International Journal of Solids and Structures 41 (2004) 44574472 .

[19] B. Li, X. Chen, J. Ma and Z. He, Detection of crack location and size in structures using wavelet finite element methods. Journal of Sound and Vibration 285 (2004) 767782.

[20] P. L. Liu and C. C. Chen, Parametric identification of truss structures by using transient response. Journal of Sound and Vibration 191(2) (1996) 273287.

[21] C. Mares and C. Surace, An application of genetic algorithms to identify damage in elastic structures. Journal of Sound and Vibration 195 (1996) 195215.

[22] A. Messina, Detecting damage in beams through digital differentiator filters and continuous wavelet transforms. Journal of Sound and Vibration 272 (2004) 385412.

[23] J. Oh, M. Cho and J. S. Kim, Dynamic analysis of composite plate with multiple delaminations based on higher-order zigzag theory. International Journal of Solids and Structures 42(23) (2005) 61226140.

[24] A. V. Oppenheim and R.W. Schaffer, Discrete-time signal processing. Englewood Cliffs, New Jersey, 1989.

[25] N. J. Pagano, Exact solution for rectangular bidirectional composites and sandwich plate. Journal of Composite Materials 4 (1970) 2034.

[26] L. Råde and B. Westergren, Mathematics Handbook for Science and Engineering. Springer, 1999.

[27] G. Rus, S. Wooh and R. Gallego, Analysis and design of wedge transducers using the boundary element method. Journal of the Acoustical Society of America 115 (2004) 29192927.

[28] G. Rus, S.Y. Lee and R. Gallego, Defect identification in laminated composite structures by bem from incomplete static data. International Journal of Solids and Structures 42 (2005) 17431758.

[29] G. Rus, S. Y. Lee, S. Y. Chang and S.C. Wooh, Optimized damage detection of steel plates from

noisy impact test. International Journal for Numerical Methods in Engineering 68(7) (2006) 707727.

[30] G. Rus, R. Palma and J. L. Pérez-Aparicio, Optimal measurement setup for damage detection in piezoelectric plates. International Journal of Engineering Science 47 (2009) 554-572.

[31] A. Saltelli, K. Chan and E. M. Scott, Sensitivity Analysis. John Wiley & Sons LTD, 2000.

[32] M. W. Suh, M. B. Shim and M. Y. Kim, Crack identification using hybrid neuro-genetic technique. Journal of Sound and Vibration 238(4) (2000) 617635.

[33] A. Tarantola and B. Valette, Inverse problems = quest for information. Journal of Geophysical Research 50 (1982) 159170.

[34] L. Westergren, Mathematics handbook for science and engineering. Springer-Heidelberg, 1999.

[35] W. X. Yang, J.B. Hull and M.D. Seymour, A contribution to the applicability of complex wavelet analysis of ultrasonic signals. NDT E International 37 (2004) 497504.